A&A 388, 29–49 (2002)
DOI: 10.1051/0004-6361:20020432

Astronomy & Astrophysics

Structure and stellar content of dwarf galaxies

VII. B and R photometry of 25 southern field dwarfs⋆ and a disk parameter analysis of the complete sample of nearby irregulars⋆⋆

B. R. Parodi, F. D. Barazza, and B. Binggeli

Astronomisches Institut der Universität Basel, Venusstrasse 7, 4102 Binningen, Switzerland

Received 23 January 2002 / Accepted 12 March 2002

Abstract. We present B and R band surface photometry of 25 Southern field dwarf galaxies within a distance of 10 Mpc. For each galaxy we give the essential model-free photometric parameters and, by fitting exponentials to the surface brightness profiles, the central extrapolated surface brightness and the exponential scale length, in both colour bands. Surface brightness and colour profiles are shown. One of the objects, a very faint dwarf elliptical in the vicinity of NGC 2784, has been discovered in the course of this work.
Drawing on the data from this and all previous papers of this series, we construct a complete sample of 72 late-type ("irregular") dwarf galaxies in nearby groups and the field within the 10 Mpc volume, to study the exponential-disk parameter relations of these galaxies with respect to galaxy environment. We confirm our previous finding of statistically lower scale lengths/higher central surface brightnesses for field and group galaxies as compared to cluster galaxies. However, using a clear-cut definition of "group" versus "field" environment, we find no significant difference in the photometric structure of group and field irregulars. A difference in the star formation history may partly account for this structure-environment relation: for a given luminosity cluster dwarfs are on average redder than field and group galaxies. We also report evidence for the colour gradients of dwarf irregulars being roughly inversely proportional to the disk scale lengths.
Supplementing our photometric data with kinematic data from the literature, we study possible relations with kinematic properties of the inner disk. Applying the dark matter scaling relations for a Burkert halo we show that for field and group galaxies of a given luminosity faster-than-mean disk rotational velocities at a radius of about two scale lengths are correlated with larger-than-mean disk scale lengths.

Key words. galaxies: general – galaxies: fundamental parameters – galaxies: irregular – galaxies: photometry – galaxies: structure – galaxies: kinematics and dynamics

1. Introduction

Dwarf galaxies are, aside from star clusters, the most simple and fundamental stellar systems. Their study is relevant for some of the most important problems of current astronomy, such as star formation, galaxy evolution, and dark matter. Dwarf galaxies are also the most numerous large stellar systems. Yet surprisingly, we still have a very incomplete knowledge of nearby dwarf galaxies, other than the Local Group (LG) members, in spite of the fact that the local volume, out to a distance of several Mpc, constitutes the only "fair sample" of the universe we have. Only nearby can we hope to study the very faintest galaxies, and thus, e.g., also determine the cosmologically important faint end of the luminosity function (LF). The reason for this lack of knowledge is the general *low visibility* of dwarf galaxies due to their low surface brightness and the fact that the *whole sky* has to be surveyed.

An early attempt to list all galaxies out to a LG-centric velocity of 500 km s^{-1}, corresponding roughly to a distance of 10 Mpc, by Kraan-Korteweg & Tammann (1979) has set the scene for all later efforts, including the present work, to improve on our knowledge of dwarf objects in that "10 Mpc volume". The most recent update of the "10 Mpc Catalogue", listing some 300 galaxies, is given by Karachentsev et al. (1999). Many of these objects have only recently been discovered by Karachentseva & Karachentsev (1998) and confirmed to be nearby dwarfs

Send offprint requests to: B. R. Parodi,
e-mail: parodi@astro.unibas.ch

⋆ Based on observations collected at the European Southern Observatory, La Silla, Chile.

⋆⋆ Table 3 containing "BR photometry and kinematic data for the 72 irregular dwarf galaxies of our complete sample" is only available in electronic form at the CDS via anonymous ftp to cdsarc.u-strasbg.fr (130.79.128.5) or via http://cdsweb.u-strasbg.fr/cgi-bin/qcat?J/A+A/388/29

by Huchtmeier et al. (2000). The number of known galaxies within the 10 Mpc volume is bound to grow further in the future.

Follow-up work on the known nearby dwarfs, done primarily by Karachentsev and collaborators, has mainly focused on the distance determination for these objects from the brightest blue stars in late-type, and the tip of the red giant branch in early-type dwarfs (see Karachentsev et al. 1999 and refs. therein; Seitzer et al. 2001). In order to secure also a data base of *surface photometry* for these objects, we have started a programme of systematic CCD imaging, in at least two colour bands, of all known dwarf galaxies in the 10 Mpc volume for which no such photometric data was, or is, available. Our goal is not only to contribute to the "fair sample" census mentioned above, but to study the systematic structural differences of dwarf galaxies in different environments. Clearly, the low-mass, low-density "dwarf" galaxies are expected to show the strongest reactions to, and hence the most significant signs of, environmental influences. A large and homogeneous sample of nearby, well-resolved dwarfs will therefore provide an ideal test bed for evolutionary scenarios.

In previous papers of this series we have reported on our B and R-band observations of dwarf members of the M 81, M 101, and CVnI groups (Bremnes et al. 1998, 1999, 2000 = Papers I, III, IV) and of field dwarfs in the Northern hemisphere (Barazza et al. 2001 = Paper VI). Based on these data, supplemented by data from other studies, Bremnes (2000) did a preliminary comparison of the photometric scaling properties of nearby field and group dwarfs with those of cluster dwarfs, drawing on the cluster data of Binggeli & Cameron (1993) and Ferguson & Sandage (1990). Bremnes (2000) found an important, significant effect: at a given total magnitude, the central exponential (or also effective) surface brightness of a dwarf galaxy – of early *or* late type – is lower in the high-density environment of a cluster than in the low-density field or group. The same trend is mirrored in the exponential scale length or the effective radius. A sample of Northern field dwarfs was added by Paper VI, where the analysis of Bremnes (2000) was repeated and his results confiremd for late-type dwarfs.

In the present paper, number VII of the series, we present, in a first part (Sect. 2), B and R-band surface photometry for another 25 Southern field dwarfs. One of these objects, now called NGC 2784 DW1, was not listed before but has been discovered on one of our images in the course of this work. As in our previous papers we show surface brightness and colour profiles and give the conventional photometric parameters (total magnitudes, effective, and exponential parameters) for all objects.

As most dwarfs in the nearby field, including groups of galaxies, are low-luminosity spirals (Scd, Sd, Sm) and irregulars (Im, BCD), we have by now accumulated a fairly large sample of late-type dwarfs. In the second part of the paper (Sect. 3) we therefore present a statistical analysis of the photometric, but also kinematic, properties of all 72 odd late-type dwarfs (= "irregulars" for short) for which we have done imaging so far. For the sake of homogeneity, the whole analysis is restricted to our own photometric data. This is in contrast to Bremnes (2000) and Paper VI, where data from the literature were mixed in.

One novelty of the present study is the use of a rather simple but clear-cut definition of "group" versus "field" dwarfs: a "field" dwarf has no neighbour brighter than $M_B = -17.5$ mag within a distance of 1 Mpc. Distance estimates are mostly provided by Karachentsev et al. (1999). In this way certain traditional group members lying in the outskirts of the group would become "field" dwarfs, and certain dwarfs satellite to giants outside of the known groups would become "group" dwarfs. A similar but continuous, and more physically motivated environmental parameter, the "tidal index", was introduced before by Karachentsev & Makarov (1999).

We confirm, in Sect. 3.4, that there is a significant shift in exponential scale length, and consequently in all other photometric parameters as well, at a given total magnitude, between field and group and cluster irregulars; there is, however, no such shift between group and field objects alone. There is some support for Bremnes' (2000) interpretation of this effect in terms of a difference in star formation history, in that the higher surface brightness field and group irregulars are also bluer. However, the photometric difference between field/group and cluster dwarfs could primarily also be a *structural* difference: in a cluster environment the dwarfs could plausibly have been puffed up to larger scale length by frequent tidal encounters. Moreover, different halos in different environments may also cause a shift: by combining our photometry with H I rotational velocity data from Karachentsev et al. (1999) and that for the PGC (Bottinelli et al. 1990), in Sect. 3.6, we show that our irregulars are indeed rotating disk galaxies obeying a Tully-Fisher relation, and that photometric parameters are correlated with inner disk circular speeds.

We also report, in Sect. 3.5, perhaps the first clear evidence of a relation between colour gradient and exponential scale length, which has a simple physical meaning. A summary of our results can be found in Sect. 4.

2. Photometry of southern field dwarfs

2.1. Sample and imaging

The two main sources of the present photometric sample of dwarf galaxies are the catalogue of nearby galaxies by Schmidt & Boller (1992) and the list of galaxies by Karachentsev et al. (1999). Both include galaxies with a distance limit of roughly 10 Mpc. We selected 25, mostly field dwarf candidates in the southern sky from these catalogues. Since some of the dwarfs are rather close companions of giant galaxies, they are not as isolated as might be associated with the definition of field galaxy. However, all but one galaxy do not belong to one of the known groups in the volume in question and are therefore defined as field dwarfs. Most of the candidates are late type galaxies. A list of the objects selected and observed along with some

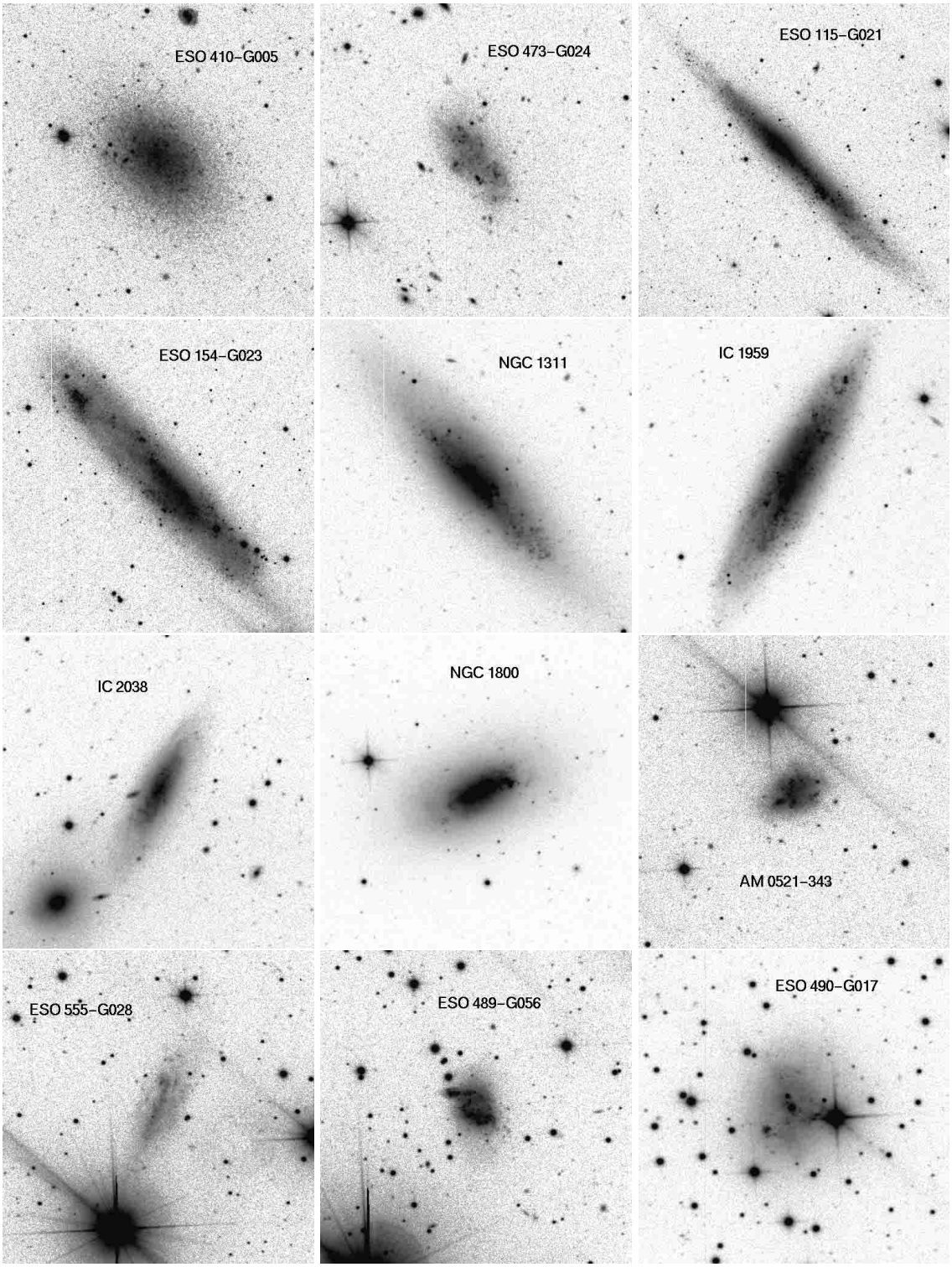

Fig. 1. B-band CCD images. Image size: $3\farcm3 \times 3\farcm3$, except for ESO 115-G021 and ESO 154-G023, for which the size is $6\farcm6 \times 6\farcm6$. North is up and east to the left.

basic data is given in Table 1. The columns of Table 1 are as follows:

Columns 2 and 3: identification of the observed galaxy;

Cols. 4 and 5: their 2000.0 epoch coordinates (from NED);

Col. 6: morphological type in the classification system of Sandage & Binggeli (1984);

Col. 7: galaxy semi-major (R_{25}) and semi-minor axis (r_{25}) in arcsecs and at the level of 25 mag/$\Box''$; used as ellipse fit parameters;

Col. 8: position angle at the level of the 25 mag/$\Box''$ isophote, measured from north to east;

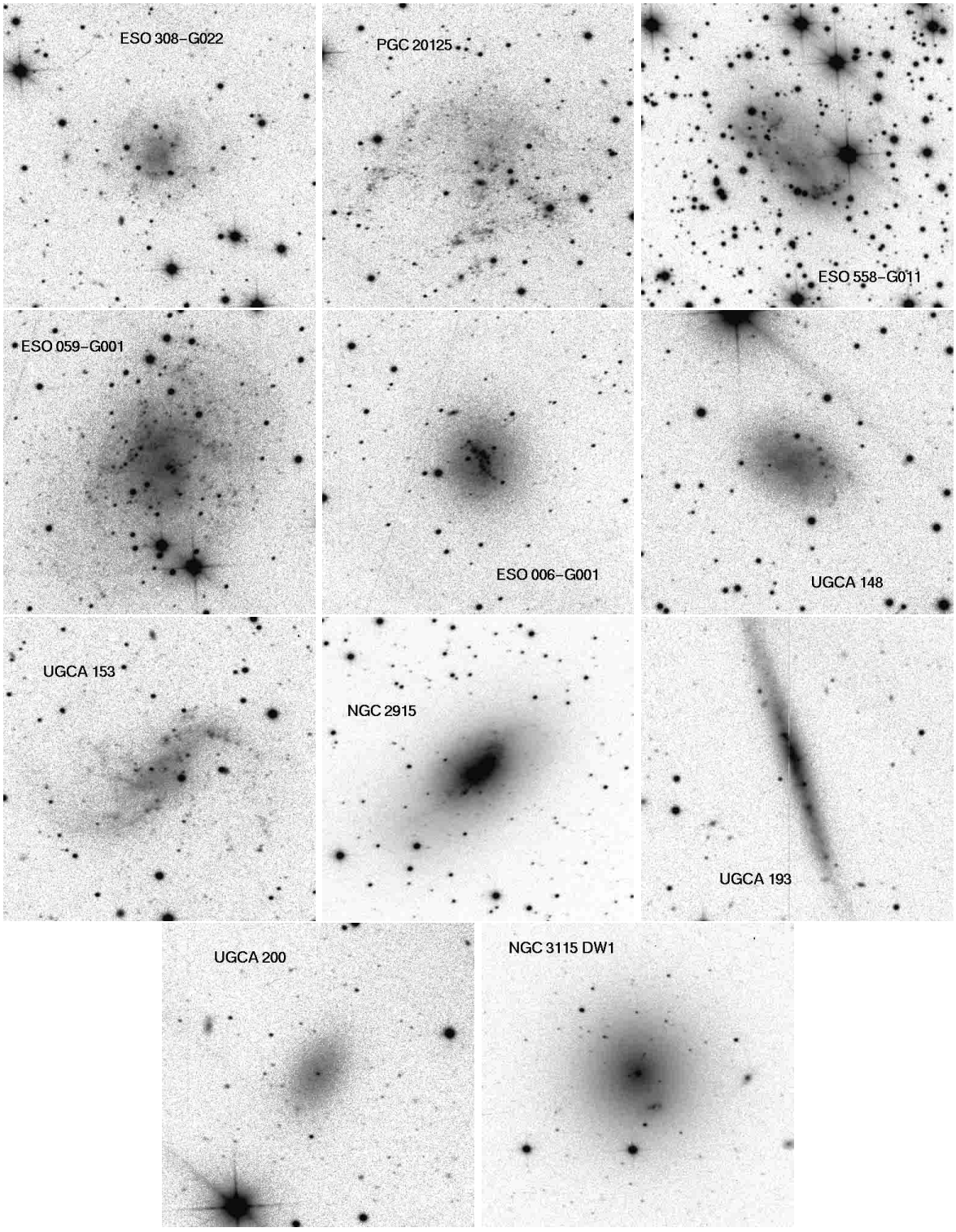

Fig. 1. continued.

Col. 9: total B-band magnitude, corrected for galactic extinction (cf. Table 2);
Cols. 10 and 11: heliocentric radial velocity in $\mathrm{km\,s^{-1}}$ (from the NED) and distance in Mpc (mostly from Karachentsev et al. 1999 and Huchtmeier et al. 2000; see also Sect. 3.1);
Col. 12: absolute B-band magnitude, based on the data given in Cols. 9 and 11.

Distances are available from the catalogues of Karachentsev et al. (1999) and Huchtmeier et al. (2000) for all but one of the observed galaxies. These distance estimates are based on the luminosity of the brightest blue

Table 1. Basic data of the observed dwarf galaxies.

No. (1)	Ident. 1 (2)	Ident. 2 (3)	RA (4)	Dec (5)	Type (6)	$R_{25} \times r_{25}$ (7)	PA (8)	B (9)	$V_{\rm hel}$ (10)	Dist. (11)	M_B (12)
1.	ESO 410-G005	KK 3	00 15 31.13	−32 10 55.46	dE	37.0×25.4	46	14.84	...	1.9	−11.55
2.	ESO 473-G024	PGC 1920	00 31 23.06	−22 46 02.30	Im	28.0×12.8	38	15.96	541	8.7	−13.74
3.	ESO 115-G021	PGC 9962	02 37 48.10	−61 20 18.00	Sm	148.5×22.2	45	13.23	513	4.8	−15.18
4.	ESO 154-G023	PGC 11139	02 56 50.38	−54 34 17.10	Sm	197.0×42.4	42	12.62	578	5.9	−16.23
5.	NGC 1311	ESO 200-G007	03 20 07.37	−52 11 06.68	Sm	93.6×27.8	41	13.09	571	5.7	−15.69
6.	IC 1959	ESO 200-G039	03 33 11.80	−50 24 38.28	Sdm	76.5×18.3	−29	13.21:	640	6.7	−15.92:
7.	IC 2038	ESO 157-G001	04 08 54.10	−55 59 31.20	Sd	52.4×15.3	−27	14.93:	712	7.6	−14.47:
8.	NGC 1800	ESO 422-G030	05 06 24.07	−31 57 10.90	Sm/BCD	60.6×34.3	−70	13.01	803	7.1	−16.25
9.	AM 0521-343	KK45	05 23 23.40	−34 34 30.00	Im	23.3×15.6	−65	15.74:	...	9.9	−14.24
10.	ESO 555-G028	PGC 18370	06 04 27.92	−19 37 20.70	Im	31.7×11.8	−26	16.01:	882	6.4	−13.02:
11.	ESO 489-G056	PGC 19041	06 26 16.98	−26 15 56.20	Im	22.9×16.5	24	15.42	495	3.7	−12.42
12.	ESO 490-G017	PGC 19337	06 37 56.60	−25 59 58.70	Im	51.9×40.5	−26	13.67:	499	7.0	−15.55:
13.	ESO 308-G022	PGC 19382	06 39 33.08	−40 43 18.50	Im	18.8×17.0	−20	15.67	821	7.5	−13.71
14.	PGC 20125	AM 0704-582	07 05 17.40	−58 31 14.00	Im	27.3×19.1	−6	14.44	554	3.8	−13.46
15.	ESO 558-G011	PGC 20171	07 06 56.84	−22 02 26.10	Im	72.0×51.4	44	12.83:	737	7.1	−16.43:
16.	ESO 059-G001	PGC 21199	07 31 18.20	−68 11 16.80	Im	71.8×51.0	−19	13.35	528	3.7	−14.49
17.	ESO 006-G001	PGC 23344	08 19 23.26	−85 08 41.10	Im	37.5×31.7	9	14.30	738	7.0	−14.92
18.	UGCA 148	DDO 56	09 09 46.54	−23 00 33.00	Im	37.9×27.1	64	14.91	725	6.3	−14.09
19.	NGC 2784 DW1	...	09 12 18.50:	−24 12 41.00:	dE,N:	17.2×9.0	−89	16.38:	...	...	...
20.	PGC 166099	KK 73	09 12 29.20	−24 14 28.00	dE,N	23.5×19.3	−60	15.50	...	6.0	−13.39
21.	UGCA 153	ESO 564-G030	09 13 12.08	−19 24 31.00	Sm	42.0×17.6	−43	15.02	765	7.0	−14.20
22.	NGC 2915	ESO 037-G003	09 26 11.49	−76 37 35.60	Sm/BCD	89.1×50.3	−50	12.01	468	5.3	−16.61
23.	UGCA 193	PGC 29086	10 02 36.00	−06 00 49.00	Sdm	92.8×10.3	17	14.67	662	9.2	−15.15
24.	UGCA 200	PGC 29299	10 05 35.20	−07 44 44.00	dE,N	23.1×13.8	−31	16.16:	...	9.2	−13.66:
25.	NGC 3115 DW1	PGC 29300	10 05 41.59	−07 58 53.50	dE,N	54.3×49.2	2	13.38	698	9.2	−16.44

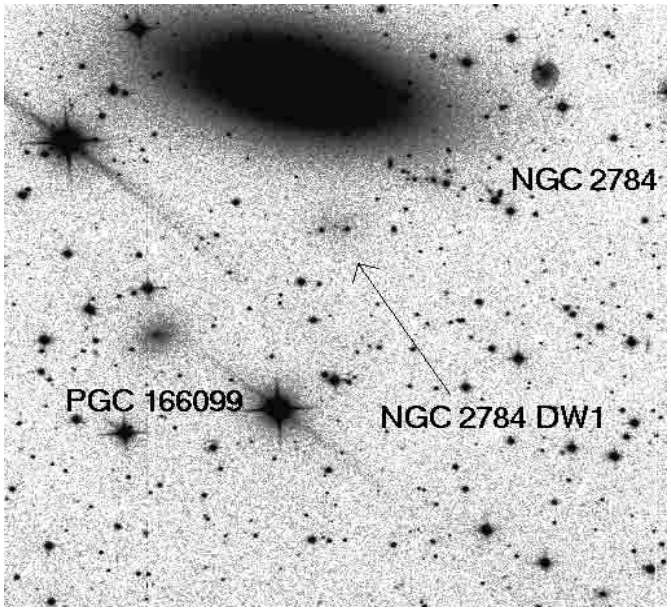

Fig. 2. B-band CCD image of the newly discovered galaxy NGC 2784 DW1, together with PGC 166099, the actual target, and NGC 2784. Image size: $9\farcm9 \times 9\farcm9$. North is up and east to the left.

stars, assumed group membership, or heliocentric radial velocity. Our galaxies are spread over almost the whole selected distance interval. NGC 2784 DW1 is a newly detected galaxy, therefore we do not have an immediate clue regarding its distance, but given its morphology (dE, N), its size and the proximity to NGC 2784 it is very likely a satellite of NGC 2784.

The mean absolute magnitude of $M_B = -14.67$ is rather bright, which is due to the fact that about a third of our galaxies have distances >7 Mpc. The brightest dwarf is NGC 2915, which is one of the two Blue Compact Dwarf galaxies in our sample. Most of the observed galaxies are classified as Im or Sm; only five are dwarf ellipticals, all being satellites of giant galaxies. ESO 410-G005 (dE or dSph), the nearest and faintest galaxy of our sample, is a possible member of the Sculptor group (see Karachentsev et al. 2000). A CCD gallery of our sample galaxies is shown in Figs. 1 and 2.

The observations have been carried out with the 1.54-m Danish Telescope at the European Southern Observatory on La Silla, Chile, between November 23, 2000 and November 27, 2000. We used the DFOSC 2048 × 2048 CCD camera. We took three 10 min exposures in B and three 5 min exposures in R, except ESO 410-G005, for which only one 30 and one 15 min exposure in B and R, respectively, has been taken. The field of view is $13\farcm3 \times 13\farcm3$ with a resolution of $0\farcs39$ per pixel. The gain was set to $0.77e^-$ per ADU, and the CCD was read out with a read-out noise of $3.11e^-$. Seeing was between $0\farcs8$ and $2\farcs0$.

2.2. Photometric procedures

The reduction of the frames and the measurements of the photometric parameters have been performed within ESO's image processing package MIDAS and follows the procedures of Papers IV and VI. The three raw images have first been combined, bias-subtracted and then flat-fielded. The flat-field frames were obtained by taking the median of several twilight flats, which we took before and after the observing runs. The background was determined by fitting a tilted plane to average intensities of frame areas unaffected by bright stars or the object itself. The same procedure was repeated to check the remaining gradient of the background. Remaining gradients of up to

0.5% can be regarded as small enough for our purpose, which we achived after one substraction.

For the calibration we used standard stars from AU. Landolt (1992). The fields with the standard stars were imaged before and after each observing block of our targets i.e. six to seven times per night. In all four nights we could observe under photometric conditions, therefore we could combine all standard stars of one night for the calibration.

The galaxy frames were then cleaned from disturbing foreground stars or background galaxies. Only the objects, for which the membership to one of these classes was obvious, were removed. Due to the similarity of certain bright, star forming regions in the irregular galaxies to foreground stars, some of these might have remained on the frames by mistake. With the available resolution, such confusions can not be avoided. However, the measured parameters can not be wrong by much, as any bright foreground stars, which really would affect the results, are easily cognizable. That the removal of bright foreground stars is important indeed was shown in Paper VI, Sect. 4.4.

After this "cleaning" we used the ellipse fitting routine FIT/ELL3 to fit an ellipse to the isophote with the surface brightness of $\sim$25 mag/$\Box''$. The center, the ellipticity and the position angle of the major axis of this ellipse were then used to integrate the galaxy light in elliptic apertures of growing equivalent radius $r = \sqrt{ab}$, where a and b are the major and minor axis of the corresponding ellipse, respectively. Plotting the obtained intensities against equivalent radius yields the growth curve (integrated light profile). From this curve all model-free parameters can be derived (see below). The behaviour of this curve at larger radii also submits another possibility to check the flatness and level of the background. A perfectly flat background with intensity zero would show up in a perfectly asymptotic growth curve, whereas remaining gradients or deviants from zero cause an always rising or suddenly decreasing curve. A slightly positive (negative) background can now be corrected by subtracting (adding) a constant to all pixel intensities in the frame. These corrections should be small compared to the substracted background intensity. In general our flat fielding and background substraction procedures worked very well, only the images taken very close to the galactic plane, which were crowded by foreground stars and where a determination of the background was difficult, suffered from remaining gradients. However, these gradients only affect the faintest parts of the galaxies and do not strongly influence the global parameters considered in this work.

2.3. Photometric parameters and radial profiles

All model-free photometric parameters can be determined on the basis of the growth-curve. Its asymptotic value yields the total intensity of the galaxy, $I_{\rm T}$, which is related to the total apparent magnitude, m, through:

$$m = -2.5\,\log(I_{\rm T}) + c. \qquad (1)$$

c is a constant derived from the calibration. m translates to B or R depending on the colour band.

The effective radius can be read off at half of the total growth curve intensity. Since we integrated the galaxy light in elliptical apertures, *a radius refers always to an equivalent radius*, if not stated separately. Together with the total apparent magnitude this yields the effective surface brightness by

$$\langle\mu\rangle_{\rm eff}\,[{\rm mag}/\Box''] = m + 5\,\log(r_{\rm eff}['']) + 1.995. \qquad (2)$$

The global photometric parameters of the observed galaxies are listed in Table 2 (left part), where *all magnitudes, surface brightnesses, and colours listed are corrected for galactic extinction* based on Schlegel et al. (1998). The columns of Table 2 represent:

Col. 2: name of the galaxy.

Col. 3: total apparent magnitude in the B band.

Col. 4: total $B-R$ colour index.

Col. 5: galactic absorption in B using the extinction maps of Schlegel et al. (1998).

Cols. 6 and 7: effective radius in B and R, respectively, in arcseconds.

Cols. 8 and 9: effective surface brightnesses in B and R, respectively, in mag/$\Box''$.

The surface brightness profiles, obtained by differentiating the growth curve with respect to equivalent radius, are shown in Fig. 3 with a resolution or bin size of $0\farcs39$, which corresponds also to the pixel size. The profiles are traced down to the radius where the growth curve becomes flat.

Beside the model-free parameters described above there are some convenient model-dependent parameters as well, namely central surface brightness, scale length, and goodness-of-fit parameter. The derived values for the individual galaxies are collected in Table 2 (right part) where the columns read as follows (again *after correction for galactic extinction*):

Cols. 10 and 11: extrapolated central surface brightness according to Eq. (3) in $B\,[{\rm mag}/\Box'']$ and $R\,[{\rm mag}/\Box'']$, respectively.

Cols. 12 and 13: exponential scale length in arcseconds ['], in B and R, respectively.

Cols. 14 and 15: difference between the total magnitude as derived from the exponential model and the true total magnitude in B and R, respectively.

The meaning of these parameters and the reason for their introduction is straightforward. Since the sample considered here consists mainly of dwarf irregular galaxies, most of the resulting profiles look rather noisy, above all in the central parts. *At larger radii* the profiles become more and more straight lines, which corresponds to an *exponential behaviour* of the intensity profile. The outer profile might represent the older, underlying stellar disk of the galaxy and therefore provides a physically meaningful parameter when fitted by an exponential function (de Vaucouleurs 1959; Binggeli & Cameron 1993). In the

Table 2. Global photometric properties and model parameters of the observed dwarf galaxies.

No.	Galaxy	B	$B-R$	A_B	$r^B_{\rm eff}$	$r^R_{\rm eff}$	$\mu^B_{\rm eff}$	$\mu^R_{\rm eff}$	$\mu^B_{0,\rm exp}$	$\mu^R_{0,\rm exp}$	$1/\alpha_B$	$1/\alpha_R$	Δm_B	Δm_R
(1)	(2)	(3)	(4)	(5)	(6)	(7)	(8)	(9)	(10)	(11)	(12)	(13)	(14)	(15)
1.	ESO 410-G005	14.84	1.02	0.06	24.20	25.55	23.75	22.85	22.67	21.55	14.56	14.52	0.02	−0.07
2.	ESO 473-G024	15.96	0.61	0.08	16.93	17.54	24.10	23.56	22.00	21.72	7.32	8.16	−0.28	−0.18
3.	ESO 115-G021	13.23	0.91	0.11	33.19	34.81	22.83	22.02	21.63	20.87	19.35	20.34	−0.03	0.00
4.	ESO 154-G023	12.62	0.82	0.07	52.98	54.49	23.23	22.48	20.10	19.75	18.66	21.28	−0.87	−0.68
5.	NGC 1311	13.09	0.89	0.09	22.00	24.00	21.80	21.10	21.74	20.59	17.50	16.79	0.44	0.27
6.	IC 1959	13.21:	0.88:	0.05	20.08:	20.35:	21.72:	20.87:	19.25	19.01	8.54	9.88	−0.61	−0.29
7.	IC 2038	14.93:	1.09:	0.05	14.10:	14.07:	22.67:	21.58:	21.63	20.57	8.68	8.62	0.01	0.06
8.	NGC 1800	13.01	0.98	0.06	14.40	16.44	20.80	20.10	21.64	20.53	15.01	15.51	0.75	0.55
9.	AM 0521-343	15.74:	0.79:	0.12	11.70:	12.07:	23.07:	22.35:	21.60	20.95	6.12	6.57	−0.07	−0.08
10.	ESO 555-G028	16.01:	0.87:	0.38	19.19:	20.51:	24.42:	23.69:	23.43	21.89	12.00	9.87	0.03	−0.22
11.	ESO 489-G056	15.42	0.68	0.28	11.55	12.15	22.73	22.16	23.01	21.82	9.59	8.86	0.68	0.35
12.	ESO 490-G017	13.67:	0.83:	0.34	22.83:	25.56:	22.46:	21.87:	21.30	20.57	13.28	14.41	0.03	0.00
13.	ESO 308-G022	15.67	0.80	0.38	25.79	23.30	24.72	23.70	23.81	22.78	15.93	14.32	0.13	0.13
14.	PGC 20125	14.44	0.74	0.51	53.32	57.34	25.07	24.49	23.75	21.97	30.67	22.51	−0.12	−0.49
15.	ESO 558-G011	12.83:	1.01:	1.60	27.10:	30.53:	21.99:	21.24:	22.08	20.64	21.42	20.49	0.60	0.27
16.	ESO 059-G001	13.35	0.96	0.63	43.47	44.24	23.53	22.61	22.20	21.17	25.21	24.86	−0.15	−0.15
17.	ESO 006-G001	14.30	1.24	0.83	20.05	23.50	22.80	21.91	22.12	21.16	13.66	16.03	0.15	0.08
18.	UGCA 148	14.91	1.03	0.72	20.01	19.91	23.41	22.37	21.40	20.35	9.47	9.40	−0.39	−0.39
19.	NGC 2784 DW1	16.38:	1.12:	0.89	20.67:	19.85:	24.95:	23.74:	23.68	22.53	12.56	12.36	−0.19	−0.18
20.	PGC 166099	15.50	1.16	0.85	19.52	20.10	23.95	22.85	23.09	21.96	12.84	13.38	0.05	−0.01
21.	UGCA 153	15.02	0.94	0.38	30.47	31.32	24.43	23.55	23.32	22.34	17.94	18.58	0.03	−0.08
22.	NGC 2915	12.01	0.91	1.18	17.20	21.91	20.18	19.80	21.26	20.22	19.60	20.37	0.79	0.58
23.	UGCA 193	14.67	0.90	0.16	16.65	17.71	22.77	22.01	21.98	21.35	10.96	12.32	0.11	0.13
24.	UGCA 200	16.16:	1.38:	0.20	17.99:	19.55:	24.43:	23.23:	23.19	22.26	10.59	12.52	−0.09	0.00
25.	NGC 3115 DW1	13.38	1.38	0.23	29.98	28.88	22.76	21.30	22.26	20.72	21.36	20.01	0.24	0.22

surface brightness (magnitude) representation this model is of the form:

$$\mu(r) = \mu_0 + 1.086\alpha r. \quad (3)$$

The extrapolated central surface brightness μ_0 and the exponential scale length $1/\alpha$ are the two free parameters of the exponential fit. The fitting range must be defined for each galaxy individually. For most of the galaxies the choice of this interval was quite obvious, for three cases however the best fitting region was hard to find (i.e. ESO 308-G022, PGC 20125, UGCA 153). In these cases we used rather large radius ranges for the fits to compensate for the fluctuations. As mentioned, the extrapolated central surface brightness and the scale length of the best-fitting exponential for the individual galaxies are listed in Table 2, while the corresponding profiles are plotted as solid lines in Fig. 3 along with the observed profiles. Note that scientists who decide to include the central portions of their profiles for the exponential fitting as well may get rather different scale lengths and central surface brightnesses.

The deviation of the observed profile from a pure exponential law is expressed by the difference Δm between the total magnitude of an exponential intensity law, given by

$$m_{\rm exp} = \mu_0^{\rm exp} + 5\,\log(\alpha) - 1.995, \quad (4)$$

and the actual measured total magnitude. This readily explains the difference Δm to be a measure for the goodness of a fit by means of an exponential intensity profile.

Before we will address questions of accuracy in more detail in the next section, a note on colour and colour profiles. The $B-R$ colours of our sample galaxies lie between 0.61 and 1.38. As expected the 20 late-type dwarfs in the sample are very different in colour compared to the five dwarf ellipticals. The mean colour for the late-types is $\langle B-R\rangle_{\rm L} = 0.90$ whereas for the dwarf ellipticals we get $\langle B-R\rangle_{\rm E} = 1.21$. The "bluest" dE is ESO 410-G005 with $B-R = 1.02$, for which the classification as dE might indeed be doubtful (see Notes on individual galaxies). Among the late-type dwarfs two are rather red: IC 2038 with $B-R = 1.09$, which is a disk galaxy seen almost edge-on and therefore reddened by the internal dust absorption, and ESO 006-G001 with $B-R = 1.24$. The latter galaxy has a rather peculiar morphology. Its central part is dominated by bright, knotty features, which, as a whole, shows even a spiral structure. This "late-type part" of the galaxy is surrounded by a spherical, dwarf elliptical-like component, which makes the classification rather difficult. For the galaxies lying close to the zone of avoidance (e.g. ESO 558-G011), the accuracy of the determined colour can not be very high, as any slight uncertainty in the correction with respect to colour will produce a large error in the "true" colour index.

$B-R$ colour profiles are shown in Fig. 4. Due to the active or recent star formation, in the inner parts, late-type dwarfs normaly show a stellar population gradient, e.g. younger and bluer stars are centrally concentrated and older and redder stars dominate the outer parts of the galaxy. Therefore, their colour indices are expected to increase with galactocentric radius. However, only eight galaxies among the late-type dwarfs show such a positive colour gradient, another eight examples have a more or less flat colour profile and four actually have a negative gradient. As the scatter in some of these profiles is rather

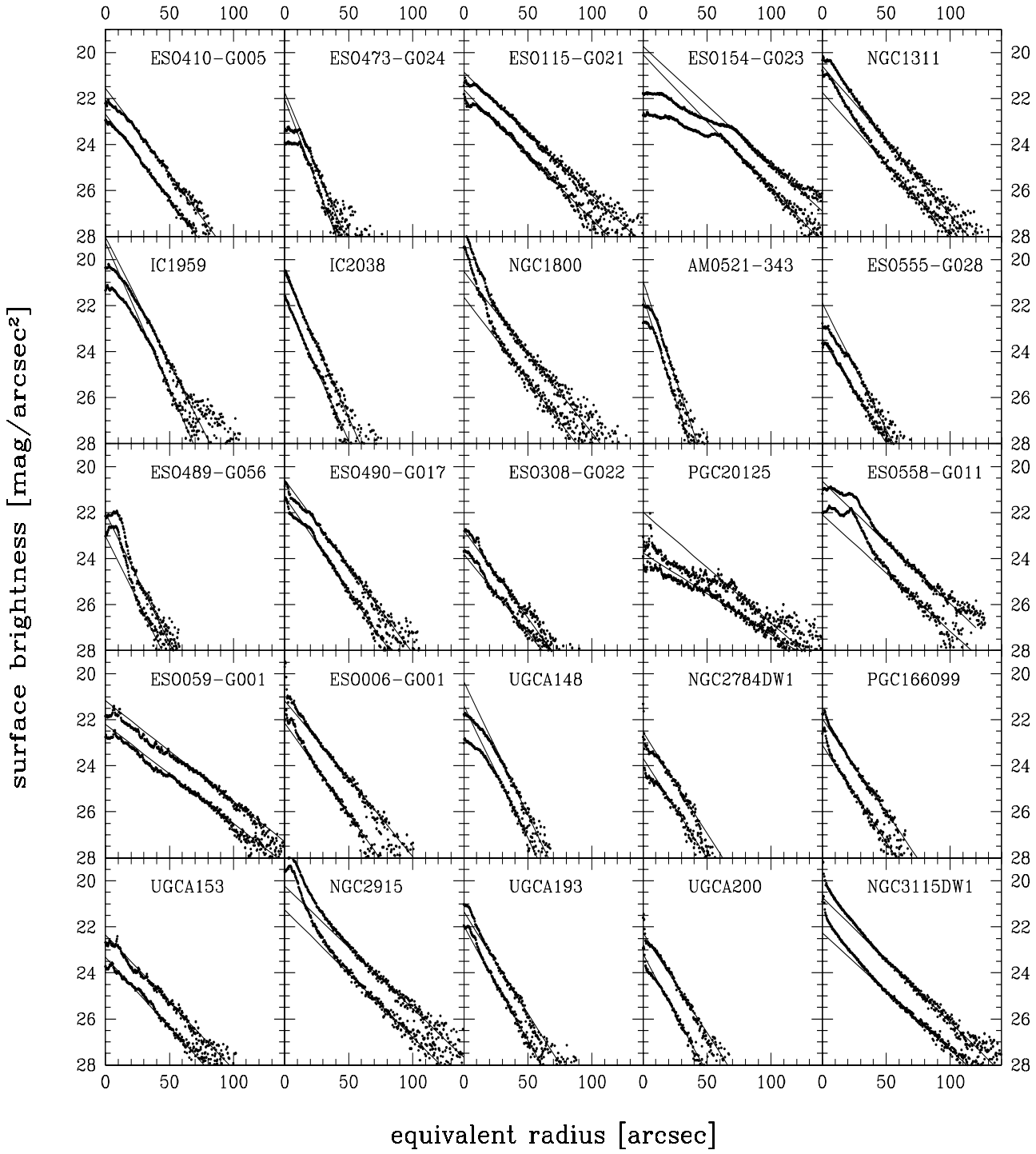

Fig. 3. Radial surface brightness profiles of the observed dwarf galaxies in B (bottom curves) and R (upper curves). The solid lines represent the exponential fits, as described in the text.

large the sign of their gradients is not obvious. Finally we remain with two clear outliers: UGCA 148 is classified as Im, but might be a transition type between Im and dE, because, aside from a couple of bright knots on the outer parts, the galaxy looks like a dwarf elliptical. UGCA 153 has clearly two spiral arms and can therefore probably be regarded as a disturbed (dwarf) spiral galaxy, hence the colour gradient makes sense.

2.4. Accuracy

The accuracy of the global photometric parameters depends of course on the correctness of the individual reduction steps and these, in turn, on the quality of the data. Apart from this the calibration represents another source of error on the global parameters. Our four observation nights have been calibrated individually by means of several standard stars. Since the whole observation could

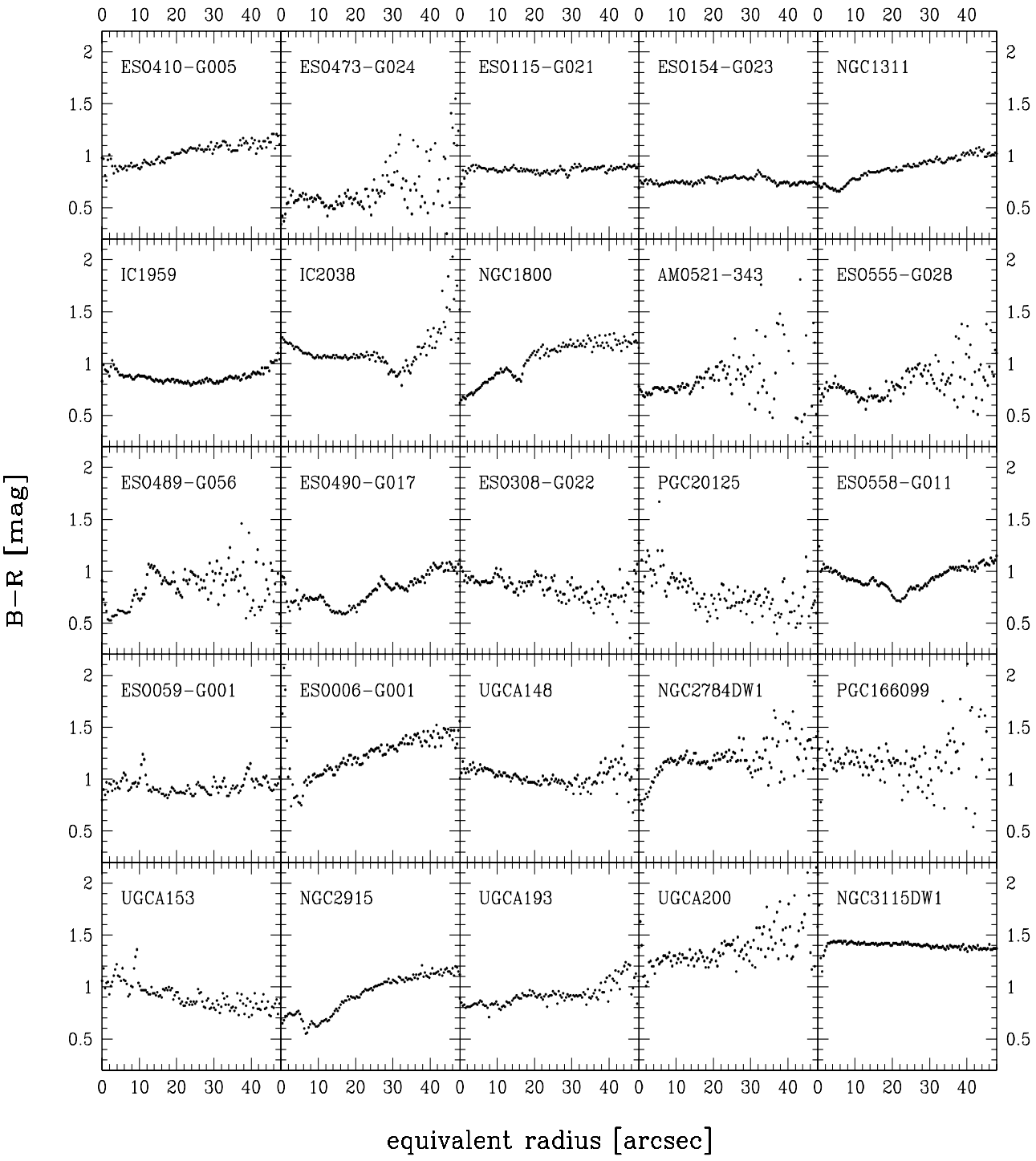

Fig. 4. Radial $B-R$ colour profiles.

be carried out under good photometric and seeing conditions, we can not only check the stability of the calibration of each night, but also compare the results of the entire run. The scatter of the obtained zero points is quite low and yields a 1σ error of 0.03 mag. Another contribution to the error comes from the determination of the extinction, which was also measured each night. The 1σ error in this case is 0.02 mag. To check the accuracy of the flat-fielding and the background substraction, we fitted a plane to the background of the already reduced image and measured the remaining gradient (see Sect. 2.2). The mean of these gradients is 0.07%, which is so low that it can be neglected. However, small fluctuations in the background can not be discovered with this method. Hints of such deviations are provided by the corrections, which have to be applied to the background in order to get a perfectly asymptotic growth curve. Only in rare cases the first integration of the galaxy light, after the standard reduction steps, yielded a

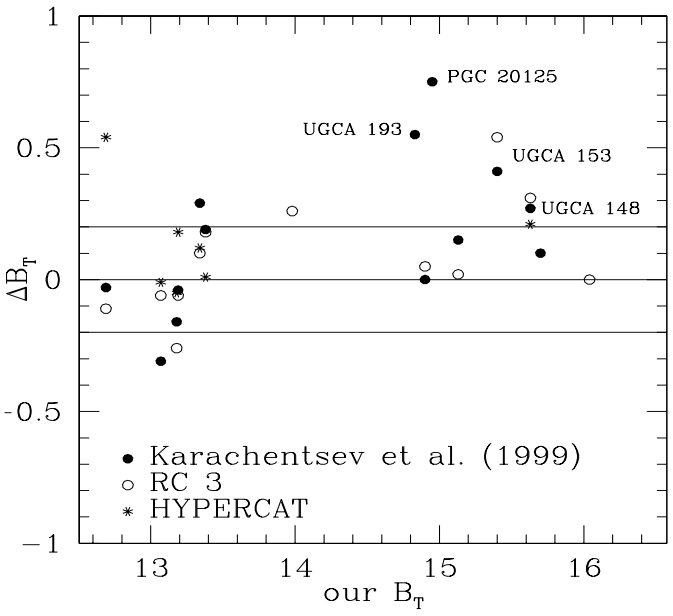

Fig. 5. Comparison of the total apparent magnitude in B (not corrected for galactic extinction) from this work with values from the literature.

perfectly assymptotic growth curve. Therefore, we normally had to correct the background by a constant, which in general was small compared to the substracted background intensity. Considering these corrections, we are on the safe side by assigning an uncertainty of 0.05 mag to this effect, which gives, together with the error from the calibration, a total error of 0.1 mag.

However, our perspective view of the objects is independent of these technical aspects of the observations, but the accuracy of the results for a galaxy beeing partly covered in projection by another galaxy or by a swarm of forground stars can not be as high as for a "isolated" object. This fact often leads to considerable differences of photometric parameters in the literature. The determined values, which are uncertain in this sense are flagged with a colon in Tables 1 and 2 and they have not been taken into account in the comparison with the parameters provided in other works shown in Fig. 5. The sources are: (1) Karachentsev et al. (1999), solid circles, who provide own results and parameters from the last version (LEDA) of the Principal Galaxy Catalogue (Paturel et al. 1992), (2) RC3 data (third reference catalogue of bright galaxies, de Vaucouleurs et al. 1991), open circles and (3) data from HYPERCAT[1], asteriks. We consider a deviation of $\leq$0.2 mag as a good agreement. What concernes the brightest galaxies our results are in agreement with at least two other sources. However, there are a few huge differences among the fainter objects. For PGC 20125 the comparison to (1) yields $\Delta B_{\rm T} = 0.75$ mag. This galaxy is very diffuse and extended and therefore difficult to measure. The deviation might be caused partly by differencies in removing forground stars. The same holds for UGCA 153 with $\Delta B_{\rm T} = 0.41$ mag to (1) and $\Delta B_{\rm T} = 0.54$ mag to (2). The difference of $\Delta B_{\rm T} = 0.55$ mag to (1) for UGCA 193 is not clear. The agreement with the actual value in LEDA is much better, $\Delta B_{\rm T} = 0.25$ mag, supporting our result. For UGCA 148 (DDO 56) the three other sources agree very well ((1): $B_{\rm T} = 15.36$ mag, (2): $B_{\rm T} = 15.32$ mag, (3): $B_{\rm T} = 15.42$ mag), whereas our result ($B_{\rm T} = 15.63$ mag) is quite deviant, which we can not explain. Altogether, our results are in good agreement with earlier studies.

[1] `http://www-obs.univ-lyon1.fr/hypercat/`

2.5. Notes on individual galaxies

ESO 410-G005: the nearest galaxy of our sample and a probable member of the Sculptor Group (Côté et al. 1997). Since some stars are resolved and therefore must be very bright, this galaxy is probably a transition type between dwarf irregulars and dwarf ellipticals. This is also supported by the colour-magnitude diagram in Karachentsev et al. (2000), derived with the Hubble Space Telescope.
ESO 473-G024: confirmed member of the Sculptor Group (Côté et al. 1997). A contour plot in the J-band is shown in Bergvall et al. (1999).
ESO 115-G021: member of the Flat Galaxy Catalogue (Karachentsev et al. 1999). It has a bulge-like feature slightly offset towards the upper left and is therefore very likely a disk galaxy seen edge-on.
ESO 154-G023: again a rather flat, but bright galaxy. The exceptional shape of the surface brightness profile is caused by the remarkable bright star forming region near the upper left edge of the galaxy.
NGC 1311: disk galaxy viewed almost edge-on. No signs of spiral arms, but obviously with a bulge. The colour profile shows a blue gradient in the central part and a reddening in the outer parts.
IC 1959: irregular disk galaxy without bulge. Again a blue colour gradient in the inner parts, more extended than NGC 1311 and probably caused by internal extinction due to dust, and a reddening towards larger radii.
IC 2038: since Karachentsev et al. (1999) do not provide a distance for this galaxy, we can only rely on its radial velocity, which is $v_{\rm hel} = 712\,{\rm km\,s^{-1}}$. However, as to its morphology and angular size the distance can not be much larger than 10 Mpc. The galaxy in the lower left is IC 2039, classified as S0. Ferguson & Sandage (1990) include it, together with IC 2038, in the Dorando Group at a distance of $\sim$20 Mpc, despite its radial velocity of $250\,{\rm km\,s^{-1}}$. In fact, the correctness of this velocity is somewhat doubtful. If it would be confirmed, the distance of IC 2039 ought to be much smaller and we would deal with a M32-like galaxy.
NGC 1800: this galaxy is undergoing a strong starburst, which is reflected in the bright bar. The $B-R$ colour map in Fig. 6 shows that the bluest, and hence strongest, star forming region is not located at the center of the galaxy, but completly offset at the end of the bar. This starburst region is also showing up in the colour gradient, which

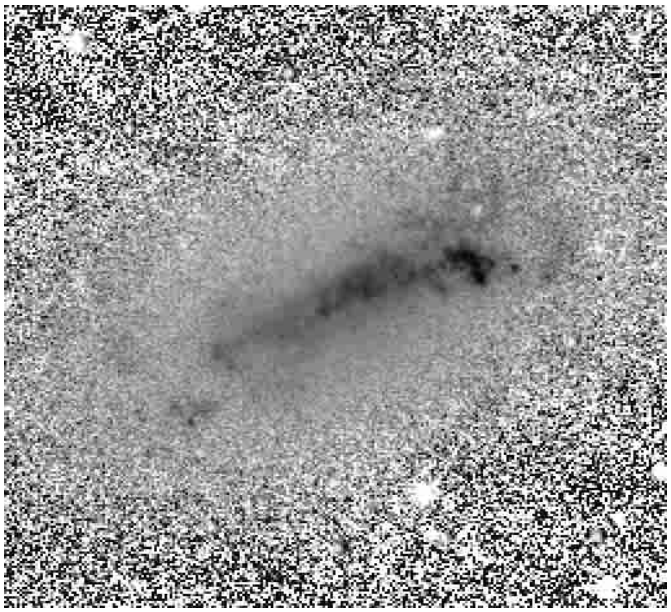

Fig. 6. $B-R$ colour map of NGC 1800. Shown is the interval 0.3 (black) $\leq B-R \leq$ 1.7 (white). The image size is $1'.65 \times 1'.65$. North is up and east to the left.

suddenly decreases at $r \sim 12''$. Marlowe et al. (1999) include this galaxy in their sample of blue amorphous galaxies and examine its taxonomy and starburst properties.

AM 0521-343: peculier shape and many bright starforming regions asymetrically distributed.

ESO 555-G028: rather diffuse and faint galaxy with a bar and an oscillating colour gradient.

ESO 489-G056: the fuzzy object at the upper left of the galaxy is a background spiral. The galaxy has a peculier shape, the starforming regions being concentrated in the lower part. Kunth & Östlin (2000) include it in their list of the most metal-poor galaxies.

ESO 490-G017: a bright starforming region is visible in the lower left of the galaxy, another such region might be covered by the bright star on the right side of the galaxy. The two bright objects near the center are foreground stars.

ESO 308-G022: dwarf irregular galaxy with only a few bright regions and an extended and diffuse outer part.

PGC 20125: Very peculier shape. The galaxy is extended and has almost no compact region.

ESO 558-G011: this galaxy is located close to the galactic plane and therefore crowded with foreground stars. The colour profile is v-shaped: the galaxy becomes bluer from the center to the starforming regions and then reddens again towards the edge.

ESO 059-G001: a dwarf irregular galaxy with rudiments of spiral arms.

ESO 006-G001: this galaxy shows a considerable reddening in its colour profile. In fact, the envelope is very similar to a dwarf elliptical and the surface brightness profile is almost perfectly exponential in this part. The center is dominated by two engulfed chains of bright knots. A transition type between dwarf irregular and dwarf elliptical?

UGCA 148: the galaxy has a decreasing colour gradient (see Sect. 2.3). With the exception of the brighter regions at the right edge, the galaxy is very diffuse and uniform. It is probably a transition type between Im and dE. This is also supported by recent radio observations by Simpson et al. (2000), who find only a small amount of HI gas.

NGC 2784 DW1 and PGC 166099: in the field of our target object PGC 166099 we discovered another very faint galaxy, which we call NGC 2784 DW1. Figure 2 shows a B-band CCD image of the two dwarf galaxies together with the Sa galaxy NGC 2784. Neither the NED nor the LEDA data bases list any object at this position. In view of the size and the visiual appearance of NGC 2784 DW1 on our image we suggest that it is another companion of NGC 2784. Two bright stars lie in front of the galaxy, covering a substantial part of its image. We consider the fainter object near the center as the nucleus of the galaxy and classify it therefore as dE,N. Adopting the distance of NGC 2784 we get an absolute magnitude of $M_B = -12.40$, which is rather faint for a dE,N. PGC 166099 (KK 73) appears in the list of Karachentsev et al. (1999) and is clearly a dE,N. Its distance has not been measured directly, but it is also considered to be a satellite of NGC 2784.

UGCA 153: since the galaxy is quite isolated the striking feature on the upper part is most likely some kind of spiral arm rather than a tidal tail. There is also a rudiment of another arm on the opposite side. The colour gradient also supports the suggestion that this object might be a (disturbed) dwarf spiral (see Sect. 2.3).

NGC 2915: this is the brightest galaxy in the La Silla sample with $M_B = -16.61$. There are many contributions in the literature for this galaxy, which is commonly classified as a blue compact dwarf, but with a very extended HI disk, which even shows some traces of spiral structure (see Bureau et al. 1999). An optical study is presented in Meurer et al. (1994). Like for NGC 1800 the colour gradient indicates that the brightest star forming region is offset.

UGCA 193: a disk galaxy seen perfectly edge-on. The measured colour of $B-R = 0.90$ might be an overestimate due to some internal extinction. The galaxy is also a member of the Flat Galaxy Catalogue (Karachentsev et al. 1999). Haynes et al. (1998) present a 21 cm HI line profile, which clearly shows that the galaxy is rotating.

UGCA 200: this dE,N is a faint companion of the S0 galaxy NGC 3115. Not surprisingly for a dwarf elliptical it is very red, $B-R = 1.38$, and has a rising colour gradient.

NGC 3115 DW1: this galaxy, another companion of NGC 3115, is a typical dE,N, very bright and very red. An analysis of its Globular Cluster system, based on HST observations, is presented in Puzia et al. (2000). They also include an image from the Digitized Sky Survey, which shows the relative position of the dwarf and NGC 3115. Also visible, but not marked, is UGCA 200.

3. Disk parameter analysis of the complete sample of dwarf irregular galaxies

Our long-term project of establishing a volume-limited data base on the photometry of nearby dwarf galaxies is approaching its final stage. We may now proceed with the exploitation of the accumulated information. Earlier analyses have already revealed a new effect which needs to be confirmed. With our larger, nearly complete sample at hand we may hope to find other interesting relations among the parameters available. *Concerning photometry the present analysis focuses on exponential parameters of dwarf irregular galaxies.* Where not stated separately the term "irregular" denotes all late-type dwarfs, i.e. Im galaxies, BCD or BCD-like galaxies as well as spirals of type Scd or later. More photometric parameter relations, including dwarf elliptical galaxies, are discussed in Bremnes (2000).

3.1. The complete sample

In a series of five papers (Papers I, III, IV, VI, and this one) we have presented photometric results for more than 100 field and group dwarf galaxies in the nearby 10 Mpc volume. Among the galaxies with reliable distance estimates there are 71 dwarf irregulars with B- and R-band data and 4 with B-band data only. Three galaxies (UGC 5658, UGC 8914, and DDO 97) with distances clearly above 10 Mpc are excluded in the following. The three galaxies with the largest distances within the sample are then BK1N at 10.5 Mpc, UGC 4998 at 11.2 Mpc and Kar54 at 12.2 Mpc.

BR photometry and kinematic data for 72 irregular dwarf galaxies of our sample are listed in Table 3 (available only in electronic form at the CDS, see footnote on first page). Selected columns are taken over from our series of papers, complemented where necessary, converted to physical units where adequate, and two columns are newly added. The meaning of the individual columns is as follows:

Column 1 gives the reference to the original publication. Roman numbers refer to the papers of our series with VII being the present one. Columns 2 and 3 name the galaxy and its type. Columns 4 and 5 list the B apparent magnitude (corrected for galactic extinction) and $B-R$ colour, while Col. 6 gives the B absolute magnitude calculated by means of the distance in Col. 7. With a few exceptions all the distances are from the catalog of nearby galaxies by Karachentsev et al. (1999) and given in Mpc; they are based on photometric, group-membership and Hubble law distance determinations. For five galaxies (KK45, ESO 555-G028, ESO 489-G056, ESO 308-G022, and ESO 558-PN011) Hα distance estimates are taken from Huchtmeier et al. (2000), and for seven galaxies (Kar54, UGC 4998, BK1N, NGC 4248, ESO 473-G024, IC 2038, and ESO 059-G001) distances are determined in accordance with Karachentsev et al. (1999) by means of a Local Group centroid correction and of the Hubble law using a local Hubble constant of $H_0 = 70$ km s^{-1} Mpc^{-1}.

Column 8 informs about field (F) or group (G) membership. While most galaxies in Papers I, III, and IV were considered to be group galaxies and those in Paper VI to be field galaxies, we apply a common selection criterion to the galaxies of the present study: *we define a group dwarf galaxy as one with a neighbour brighter than -17.5 in absolute magnitude and with a relative distance of less than 1 Mpc.* As a pool for possible neighbouring galaxies the catalog of Karachentsev et al. (1999) was used which provides distance information for more than 300 galaxies within 10 Mpc.

Column 9 lists the axial ratio of the fitted ellipse at the 25th-mag/arcsec^2 isophote. Columns 10 and 11 give the B-band model parameters for an exponential light distribution, i.e. extrapolated central surface brightness in mag/arcsec^2 (uncorrected for inclination) and the corresponding scale length in pc (measured in terms of equivalent radii), respectively. Column 12 is a measure for the $B-R$ colour gradient (see Sect. 3.5 for an explanation), and Col. 13 lists the magnitude difference between that of a virtual comparison galaxy with a purely exponential radial surface brightness profile and that of the actual galaxy (as defined in Sect. 2.3).

Unlike in Paper VI where external data from other authors was added to enlarge the sample we will rely only on our own photometric data set. This guarantees a consistent treatment (as exemplified in Sect. 2) which is particularly required for the inquiry of subtle effects that otherwise could be overseen in an increased extrinsic scatter. However, for a comparison with dwarf irregular galaxies residing in *clusters* we will refer to the compilation of Bremnes (2000) including Virgo cluster data from Binggeli & Cameron (1993) and Centaurus cluster data from Jerjen & Dressler (1997).

Finally, in Col. 14 we compile the measured rotation velocities where available. The majority stems from Karachentsev et al. (1999), and for the other about 20 percent galaxies left the 21-cm line width measurements were taken from Bottinelli et al. (1990), corrected for turbulent motion according to the prescriptions of Tully & Fouqué (1985), and inclination corrected assuming a mean intrinsic axial ratio of $q_0 = 0.2$ on behalf of Hubble's formula for the conversion of b/a into an inclination angle (Hubble 1926) and allowing for a minimum inclination of 25°.

3.2. Luminosity function

The distance and apparent-magnitude distributions as well as the corresponding luminosity function for the 72 dwarf irregular galaxies are shown as histograms in Fig. 7. The binnings are 0.5 mag for the magnitude distributions and 0.5 Mpc for the distance distribution. The luminosity function exhibits a skewed shape which is due the different contributions of the Im galaxies, BCD or BCD-like galaxies, and the spiral galaxies. While the Im galaxies are distributed symmetrically around a pronounced peak

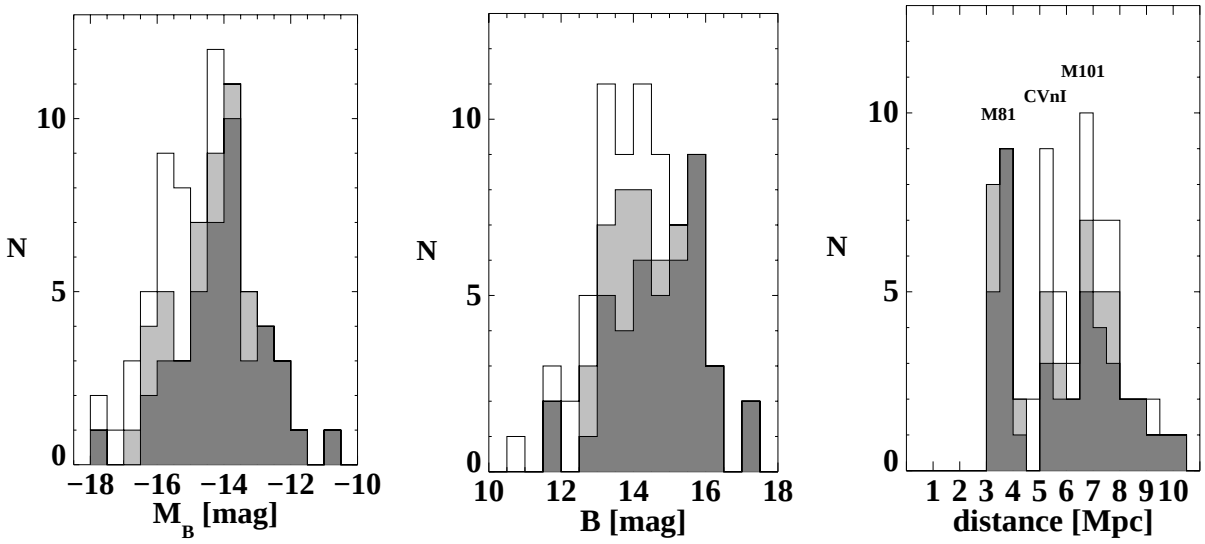

Fig. 7. Luminosity function, apparent magnitude distribution, and distance distribution for the Im galaxies (dark shaded), BCD or BCD-like galaxies (light shaded), and spiral galaxies later than Sc (white). Binnings are 0.5 mag for the magnitude distributions and 0.5 Mpc for the distance distribution.

at $M_B = -14$ mag, the brighter spiral and BCD galaxies add to the more luminous part of the distribution. The apparent-magnitude distribution shows a prominence of galaxies in the range between 13 and 16 mag with the Im galaxies providing a steadily increasing partition up to a cut-off at 16 mag. This 16 mag cut-off in apparent magnitude and the −14 mag peak in absolute magnitude combine to a distance modulus of 30 mag corresponding to our 10 Mpc volume limit. *As a limit of completeness we therefore adopt $M_B = -14$ mag; beside for explicitely stated exceptions all the following fitting procedures will rely only on data related to an absolute magnitude brighter than this.*

A peculiarity of the distance distribution is the three-peaked appearance which is basically due to the influence of the group and cloud galaxies belonging either to the M 81 group, the CVnI cloud, or the M101 group at distances around 3.5, 5, or 6.5 Mpc, respectively. The two galaxies within the sample with the largest distances are not included in the histogram.

3.3. No morphology-scale length relation

The well known relation of an increasing scale length for a brighter absolute magnitude does nicely show up in our sample, too. Free fits of the form $\log(\alpha_B^{-1}) = aM_B + \text{const}$ to the subsamples of the Im, the BCD or BCD-like, and the spiral galaxies lead to similar slopes with values $a \approx -0.10 \pm 0.03$. As can be inferred from Table 4 the three morphologically distinct constituents of our sample (Im, BCD or BCD-like, and spirals galaxies) form a homogenous data base as concerned to scale length (and consequently to central surface brightness) and to colour. The gently decreasing sequence of mean scale lengths for the subsamples at a given absolute magnitude is below statistical significance. Similarly, the mean colours

Table 4. Photometric parameter relations of dwarf irregular galaxies specified to morphology, environment, and kinematic data.

morphology	a^a	b^b	$\sigma/\sqrt{N}$	N	$B-R$	$\frac{\sigma}{\sqrt{N}}$	N
Im	-0.114 ± 0.047	1.280	0.041	21	0.98	0.05	21
BCD/ − like	-0.072 ± 0.039	1.277	0.032	9	1.02	0.05	9
late spirals	-0.099 ± 0.049	1.233	0.045	17	0.99	0.06	16
all	-0.095 ± 0.027	1.262	0.025	47	0.99	0.03	46

[a] Least-squares fits of the relation $log(\alpha_B^{-1}) = aM_B + \text{const}$.
[b] Least-squares fits of the relation $log(\alpha_B^{-1}) = -0.1M_B + b$.

environment	b^c	$\sigma/\sqrt{N}$	N	b^d	$\sigma/\sqrt{N}$	N	$B-R$	$\frac{\sigma}{\sqrt{N}}$	N
field F	1.50	0.03	32	29.68	0.18	32	0.97	0.04	31
group G	1.48	0.04	15	29.62	0.21	15	1.05	0.03	15
F&G	1.49	0.02	47	29.66	0.14	47	0.99	0.03	46
cluster[e]	1.61	0.02	81	30.18	0.24	16	...	...	...

[c] Least-squ. fits of the relation $log(\alpha_B^{-1}) = -0.08M_B + b$ ([e]).
[d] Least-squ. fits of the relation $\mu_0^{\rm B} = 0.5M_B + b$ ([e]).
[e] Slope or – in the case of the cluster galaxies – slope and intercept adopted from Bremnes (2000).

kinematic sample ($v_{\rm rot}$ known)	y^f	a	b	σ
	$\mu_{0,i}^{\rm B}$ [g]	0.79 ± 0.07	34.552 ± 1.033	1.11
	$\log(\alpha_B^{-1})^h$	-0.20 ± 0.02	-3.099 ± 0.217	0.20
	$\log(v_{\rm rot})$	-0.16 ± 0.02	-0.790 ± 0.231	0.18
	$\log(v_{\rm d})^i$	-0.15 ± 0.01	-1.035 ± 0.151	0.11
	$\log(v_{\rm h})$	-0.13 ± 0.01	-0.586 ± 0.153	0.13

[f] OLS bisector fits of the relation $y = a\,M_B + b$ to all galaxies with $v_{\rm rot}$ known ($N = 62$).
[g] Inclination-corrected central surface brightness $\mu_{0,i}^{\rm B} = \mu_0^{\rm B} - 2.5\log(b/a)$ (cf. Table 3, Cols. 9 and 10).
[h] Scale length in kpc and measured along the major axis, i.e. scale length with respect to the equivalent radius divided by $\sqrt{b/a}$ (cf. Table 3, Cols. 9 and 11).
[i] $\Upsilon = 1\,M_\odot/L_\odot^B$.

$< B-R >$ are the same within the errors to the mean of the whole sample, i.e. $< B-R >= 0.99 \pm 0.03$ mag ($M_B < -14$ mag). For our purposes we therefore see *no need to differentiate between morphological classes in the following*. Opposite to this, the galaxy environment definitely is of discriminating influence, as we will demonstrate now.

3.4. Structure-environment relation

It was recently found (Bremnes 2000; Barazza et al. 2001 (Paper VI)) that dwarf irregulars in a field or group environment have brighter central surface brightnesses in the mean than cluster dwarf irregulars. Equivalently, the scale lengths of field and group dwarf irregulars are on average lower than those of dwarf irregulars dwelling in clusters. However, comparing field against group dwarf irregulars no such differences are seen. Here we report further evidence for this trend of a structural dependence on environment among dwarf irregular galaxies.

In Fig. 8a scale length is plotted against absolute magnitude in the B band. Squares and circles represent field (50) and group (22) galaxies, respectively. The solid line is a fit to all our field (32) and group (15) galaxies brighter than -14 mag and with a forced slope of -0.08. This slope corresponds to a least-squares fit to cluster late-type galaxies in the magnitude interval $M_B \in [-13, -17]$ (Bremnes 2000) shown as the dashed line. A free fit to our dwarfs yields with values of -0.095 ± 0.027 essentially the same slope. But there obviously is a shift in the sense that – at a given absolute magnitude – *a denser environment is related to a higher scale length (fainter central surface brightness)*. Table 4 summarizes our numerical findings. While in Bremnes (2000) and in Paper VI the mean differences $\Delta\log(\alpha_B^{-1})$ were 0.15 and 0.14 ($\Delta\mu_0^B = 0.82$ and 0.76 mag), respectively, we find the shift amounting to 0.12 mag ($\Delta\mu_0^B = 0.52$ mag). Despite the lower value as compared to the previous determinations (which also included galaxies from other sources) the shift is clearly statistically significant given the uncertainty of 0.03 mag for the field and group irregulars or 0.02 mag for the cluster irregulars. Note that when comparing field and group dwarf irregulars one finds no such separation; field and group galaxies are thus not repeating the trend described above. However, the scatter σ for the (logarithmic) scale length is twice as small for the group than for the field dwarf irregulars.

The scatter – particularly for the field irregulars – is considerable and must be partly intrinsic. Given the shift between field and group and cluster galaxies we may wonder if it is related to different stellar populations dominating galaxies in different environments. Due to a lack of $B-R$ colour indices for the cluster dwarf irregulars we have to circumvent a direct $B-R$ colour comparison between the two environments. Following Bremnes (2000) we define the residuum $\delta\log(\alpha_B^{-1})$ as the difference of the measured value to the fitted value, i.e. $\delta\log(\alpha_B^{-1}) \equiv \log(\alpha_B^{-1}) - (-0.08 M_B + 1.493)$, and plotting it against colour $B-R$ some relation becomes manifest. This is revealed in Fig. 8b where a least-squares fit applied to the galaxies brighter than -14 mag (circled symbols) is shown as the solid line, obeying

$$\delta\log(\alpha_B^{-1}) = (0.16 \pm 0.12)(B-R) - 0.159\,. \quad (5)$$

Within the errors both field and group galaxies independently exhibit this same behaviour, albeit the scatter of 0.17 is considerable. Because the $B-R$ colours show no dependence on absolute magnitude M_B, *there is thus an indirect indication for a gentle but systematic trend of galaxies with higher scale lengths being redder on average and for a given absolute magnitude.*

Additionally, as indicated by the vertical lines in Fig. 8 b and as can be inferred from Table 4, group galaxies with a mean colour of $< B-R >= 1.05$ mag are on average slightly redder than field galaxies with $< B-R >= 0.97$ mag. As with scale length the scatter σ for the mean $< B-R >$ colour is smaller for the group than for the field dwarf irregulars.

3.5. Variations in the radial light distribution

The radial surface brightness profiles of most dwarf irregular galaxies (and dwarf elliptical galaxies) as well as those of spiral disks are exponentially decreasing. This is particularly true at intermediate galactocentric distances which may serve as a fitting domain. The overall accuracy of an exponential fit to a given surface brightness profile may then be quantified by the difference between the total magnitude of a purely exponential intensity law (Eq. (4)) and the actually measured total magnitude. In the previous papers of our series this quantity was named either $M_{\rm exp} - M$ or Δm (cf. Sect. 2). In Fig. 9a) Δm_B is plotted against central surface brightness μ_0^B. The majority of galaxies shows the exponential law being nominally a good description for the radial intensity distribution ($\Delta m_B \approx 0$). There are, however, quite a few aberrant galaxies. As was discussed in Paper III deviations from the exponential-fit description are frequently seen in the innermost regions and/or at large radii, the reasons ranging from strongly asymmetric distributed star formation regions to uncertain sky subtraction. Therefore it is not surprising that these deviations are not correlated with either the central surface brightness, shown here, or with other global parameters such as absolute magnitude, scale length, or colour.

The fitted exponential scale lengths provide a definition of the colour gradient in the surface brightness representation by means of differentiating Eq. (3), leading to $\nabla(B-R) \equiv 1.086(\alpha_B - \alpha_R)$. As mentioned in Sect. 2.3, and as can be seen in Fig. 9b, *most dwarf irregulars exhibit no or small, mainly positive colour gradients.* For the galaxies brighter than $M_B < -14$ mag the mean has a value of only 0.16 mag/kpc (horizontal line). Several galaxies, particularly those with small scale lengths, have strong positive colour gradients, up to

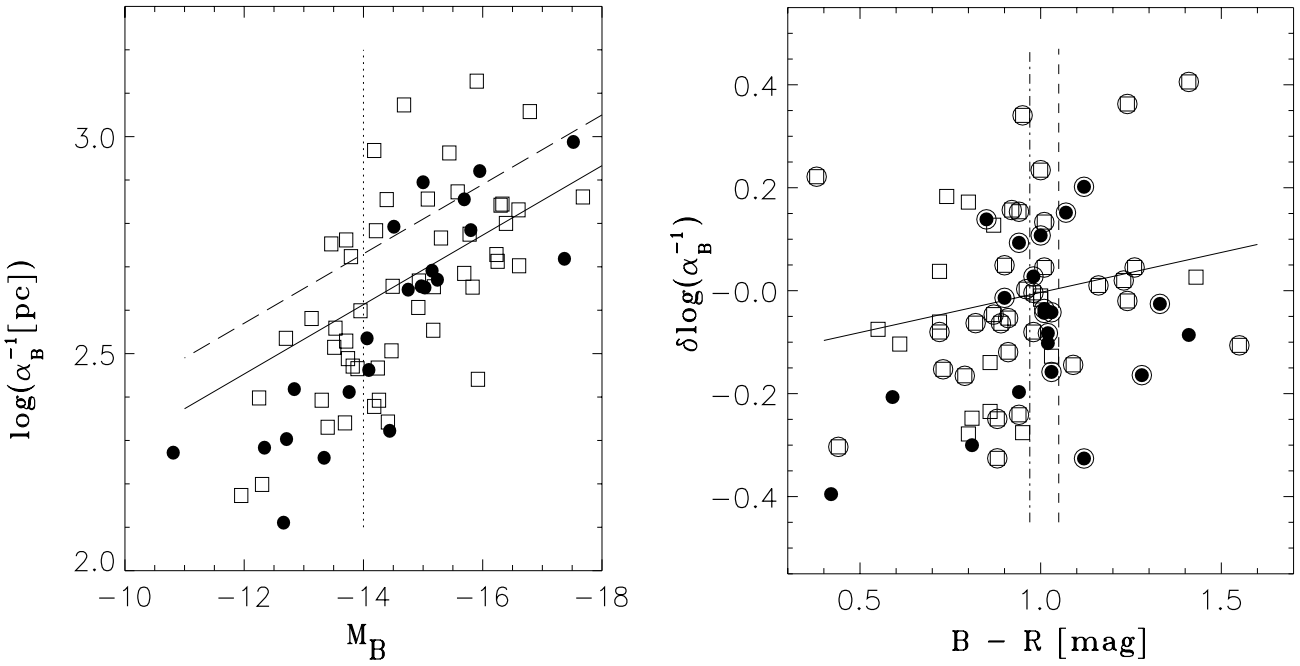

Fig. 8. a) Scale length vs absolute magnitude for the field (squares) and group (filled circles) galaxies. The solid line is a forced fit with slope −0.08 to all galaxies brighter than our limit of completeness ($M_B < -14$, indicated by the vertical dotted line). This slope was previously found for the dwarf irregular galaxies in clusters (Bremnes 2000); their corresponding relation is plotted as the dashed line for comparison. Field and group galaxies each obey the same relation (solid line). **b)** Residuum in $\log(\alpha_B^{-1})$ vs. $B-R$ colour. The residuum is defined as the difference between the measured value of $\log(\alpha_B^{-1})$ and the fitted value according to Fig. 8a. Symbols as in Fig. 8a, with those for galaxies brighter than $M_B = -14$ mag additionally circled. The solid line is a least-squares fit to these brighter galaxies only. Also indicated by vertical lines are the mean colours for the brighter field (dot-dashed) and group (short-dashed) galaxies.

more than 1 mag/kpc. This is, however, not too surprising: rewriting

$$\nabla(B-R) = 1.086(1-\alpha_B^{-1}/\alpha_R^{-1})/\alpha_B^{-1} \quad (6)$$

one immediately expects the colour gradients to be inversely proportional to the scale lengths *provided* the ratios of the blue and red scale lengths would be about constant for all galaxies. As indicated by the curved dotted line this is approximately true for most of our galaxies (drawn for an assumed proportionality $\alpha_B^{-1} = 0.9\alpha_R^{-1}$). Applying a linear relation $\alpha_B \approx 1.4\alpha_R - 0.5$ for the inverse scale lengths numerically gives a more realistic fit, including the region of negative colour gradients (short-dashed line). But this seems not to hold for a handfull of galaxies with *negative* colour gradients *and* with scale lengths shorter than about 0.6 kpc. Among them the most extremes are also faint and rather blue. However, as we will argue in Sect. 3.7.3, the colour gradients of most of these suspicious galaxies are simply inadequately determined by means of the above *deduced* gradient measure (as opposed to a gradient fitted directly to the colour profiles).

3.6. Linkage of photometric and kinematic parameters

Different models on the formation of galaxy disks all predict systematic dependencies on kinematic conditions for the resulting scale lengths and central surface brightnesses (e.g., Dalcanton et al. 1997; Weil et al. 1998; Zhang & Wyse 2000; Silk 2001). In this section we therefore seek to validate these expectations using observed quantities for the dwarf irregular galaxies of our sample. We particularly ask whether the scatter in the scale length or central surface brightness versus absolute luminosity diagram may be explained by deviating rotational velocities at fixed luminosity. In the following a variable's linear dependence on absolute magnitude defines its mean at a given luminosity. The difference of an individual data point from this mean we call the residual, in accordance to the definition given in Sect. 3.4. In Table 4 the relations for five variables are given including the particular circular velocities described below. The given relations have been determined applying *ordinary least-squares bisector fits* (Isobe et al. 1990) to all the 62 galaxies of our sample with known rotational velocity data. We chose working with bisector fits for reasons of statistical consistency: working with simple least-squares or with orthogonal fits results in spurious dependencies of the photometric variable residua on some of the photometric variables themselves. While for an exponential intensity profile the surface brightness residua have to correlate with scale length residua, other pairs of parameters should not correlate with each other. Only for ordinary least-squares bisector fits no significant correlations were found in plotting the scale length residua (surface brightness residua) against scale length (surface brightness) or absolute magnitude. This was even more

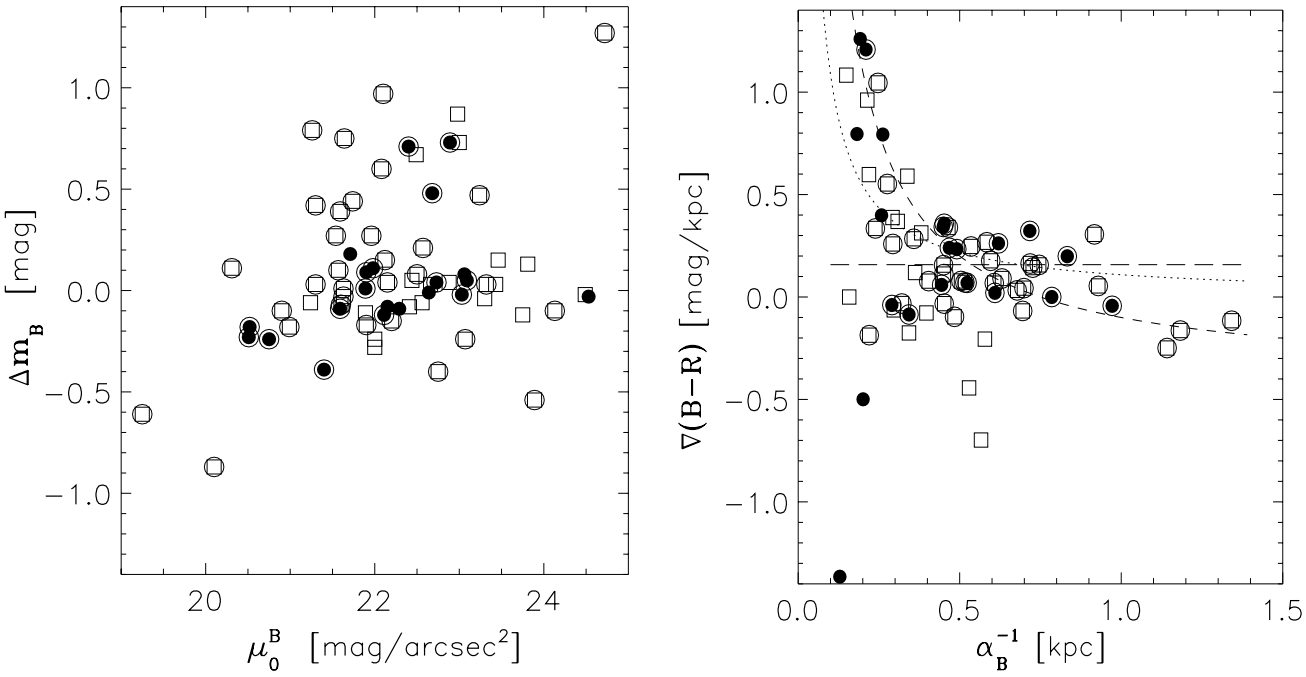

Fig. 9. a) Exponential-fit accuracy parameter versus central surface brightness in the B band. **b)** Colour gradient versus scale length in the B band. The horizontal line marks the mean for the galaxies brighter than $M_B = -14$ mag; the curved lines are proportional to the inverse scale length: the dotted one is for a constant factor of proportionality while for the short-dashed line the factor of proportionality is a linear function of scale length (see text for details). – Symbols as in Fig. 8b.

evident if *we relaxed the completeness condition*, allowing for a longer fitting intervall for the strongly scattered data in determining the mean relations listed in Table 4. Therefore we work in the following with all the galaxies for which kinematic data is available, including also the galaxies fainter than the limiting magnitude imposed so far.

A Tully-Fisher-like relation between the conventional rotational velocity $v_{\rm rot}$, measured at or beyond the optical extent of the galaxy, and absolute magnitude M_B is exhibited by the data (Table 4). Its *scatter* is rather large and, at a fixed luminosity, is *not* related to the scatter in scale length or central surface brightness. This is shown in the two leftmost residual plots of Fig. 10. And it is not surprising: dwarf irregular galaxies are known to be dark matter dominated at all radii (Carignan & Freeman 1988; Burkert 1995), thus it is not the baryonic matter that determines $v_{\rm rot}$.

A more convenient kinematic measure to work with would be given by the disk and/or halo contributions to the velocity at some characteristic *inner* disk radius. The predicted rotation curve for an exponential mass distribution corresponding to the observed exponential surface brightness profile has been analytically given for a thin, self-gravitating exponential disk (Freeman 1970). Providing a characteristic inner disk radius this description may serve here as a simple model for the luminous matter distribution and the related Keplerian kinematics despite dwarf irregular and low-surface brightness galaxies being known to be better characterized by expanded disks (Sung et al. 1998). The velocity profile exhibits a peak at radius $R_{\rm peak} = 2.14\,\alpha^{-1}$ where it has a value of $v_{\rm d} = 0.62(2\pi G\Upsilon I_0\alpha^{-1})^{0.5}$; here G is the gravitational constant, Υ the disk mass-to-light ratio, I_0 the face-on central mass surface density, and α^{-1} the scale length (e.g., Chiba & Yoshi 1995). Converted to B band observables we have

$$v_{\rm d} = 2.62 \times 10^4 \sqrt{10^{-0.4\mu^B_{0,i}}\,\alpha_B^{-1}\,\Upsilon}\ \ {\rm km\,s^{-1}} \qquad (7)$$

with $\mu^B_{0,i}$[mag/$\Box''$] the inclination-corrected central surface brightness, α_B^{-1}[pc] the disk scale length measured in parsecs along the major axis, and $\Upsilon \equiv \frac{M}{L_B}[\frac{M_\odot}{L_\odot^B}]$ the disk mass-to-light ratio in solar units. In the middle panels of Fig. 10 the deviations of this peak velocity from its mean value at a given galaxy luminosity is compared to the corresponding residuals in scale length and surface brightness. Now the two residual plots clearly suggest a linkage between photometric and kinematic properties: at a given luminosity deviations from the mean are related to different rotation velocities, in the sense that higher scale lengths or fainter central surface brightnesses correlate with *lower*-than-mean peak rotational velocites *divided* by the square root of an unknown disk mass-to-light ratio. The plots shown correspond to a constant $\Upsilon = 1\,M_\odot/L_\odot^B$. There are several caveats with our finding: First, the issue of the unknown individual mass-to-light ratios is a non-trivial one and its possible relation with surface brightness, luminosity, or color is not tackled in the above approach. Second, one must be cautious in applying the model parameter $v_{\rm d}$ which is deduced from photometric quantities only and which does not relate to an independent, actually observed kinematic quantity. Finally, the

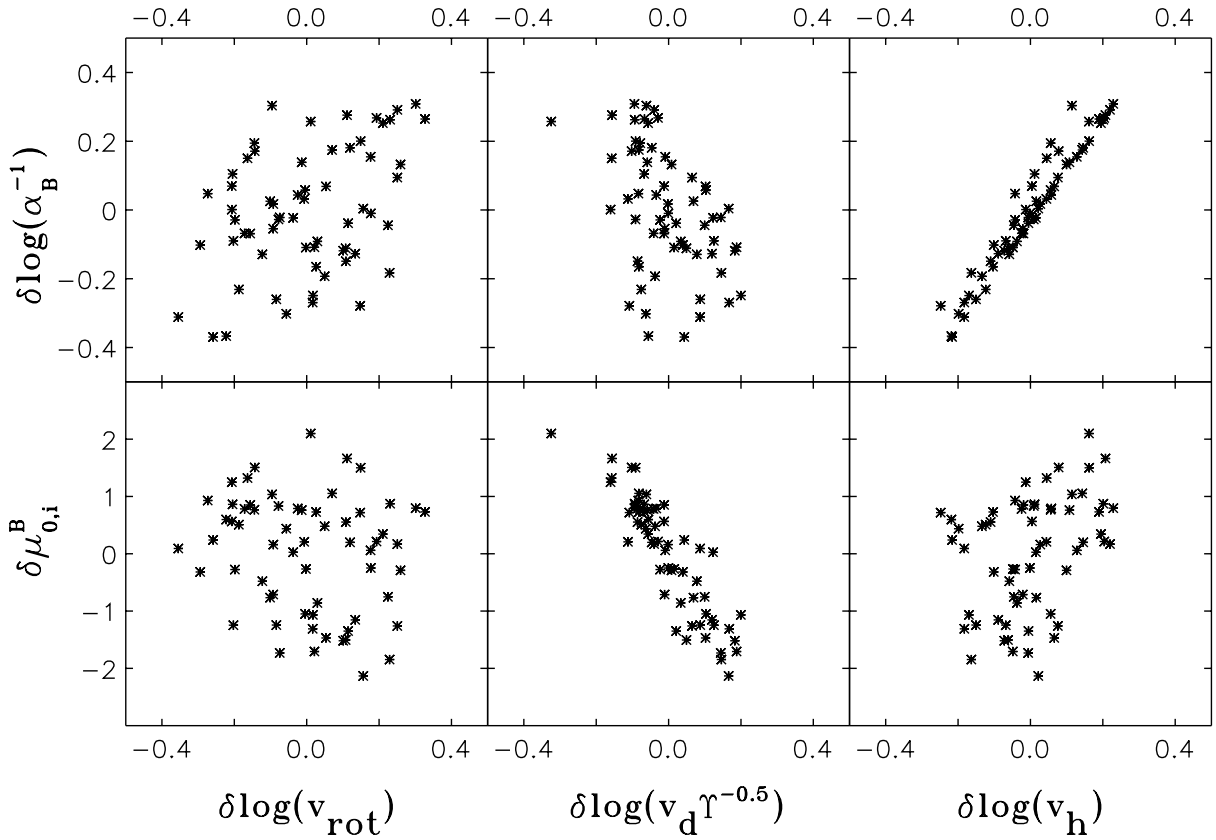

Fig. 10. Residual plots revealing the linkage of photometric with kinematic properties. The residuals for a parameter are defined as the deviations from a mean at given luminosity, while the mean is determined from an ordinary least-squares bisector fit of the parameter to absolute magnitude (see Table 4). Plotted are the residuals for scale length and surface brightness versus the residuls of three distinct circular velocities: the two leftmost panels use the residuals of the conventional rotational velocity $v_{\rm rot}$, measured at or beyond the optical extent of the galaxy; the middle panels use the residuals of the peak circular velocity of a hypothetical self-gravitating exponential disk, at an inner disk radius of about two scale lengths (Eq. (7)); and the rightmost panels use the residuls of the halo contribution to the rotational velocity at the same inner disk radius, as inferred from the Burkert (1995) halo model for dwarf irregular galaxies. See text for details.

thin disk assumption and, above all, ignoring the presence of dark matter leaves the model rather unrealistic.

However, we may approximately infer the contribution of the dark-matter halo to the total rotational velocity at $R_{\rm peak} = 2.14\,\alpha^{-1}$ (in fact, at any radius) on purely phenomenological grounds. The total rotational velocity $v(r)$ is conventionally decomposed into a dark matter ($v_{\rm h}(r)$), a stellar ($v_{\rm d}(r)$), and an HI component. Burkert (1995) and Salucci & Burkert (2000) successfully describe the rotation curves of dark matter-dominated dwarf galaxies by means of an empirically found one-parameter family of halos: Provided the rotational velocity v_0 of the dark matter halo is known at a particular density scale radius (corresponding to the halo core size of typically four to seven optical scale lengths), then the rotational velocity due to the halo $v_{\rm h}(r)$ is calculable at every radius r. One can show that the seven selected dwarf galaxies of Burkert (1995) obey $< v_0/v_{\rm rot} > = 0.78 \pm 0.05$, i.e., the input parameter v_0 typically is lower by about 20 percent than the measurable circular velocity $v_{\rm rot}$ of the flat or nearly flat part of the rotation curve. Thus we may adopt $v_0 \approx 0.78\ v_{\rm rot}$ as a working approximation and determine the halo contribution to the rotational velocity at $R_{\rm peak}$, $v_{\rm h} \equiv v_{\rm h}(R_{\rm peak})$, by means of the Burkert-halo parametrization. The rightmost panels of Fig. 10 plot its residuals versus the residuals in scale length and surface brightness. It is revealed that *the photometric exponential-disk parameters do indeed correlate with the corresponding halo-related kinematics: at a fixed luminosity higher-than-mean halo-induced rotational velocities are related to larger scale lengths and fainter central surface brightnesses.* Note, however, that there is an island of nine galaxies with lower-than-mean scale lengths and with corresponding slower-than-mean circular velocities but with central surface brightnesses too faint instead of too bright; they all are brighter than about $M_B = -16$ mag but, as far as we can tell, share otherwise no distinctive feature.

3.7. Discussion

3.7.1. Is the structure-environment relation significant?

No morphology-structure relation was surfacing from the data; the $\log(\alpha_B^{-1}) - M_B$ relations were similar for Im,

BCD/-like, and late spiral galaxies, the individual free-fit slopes yielding -0.1 ± 0.03 (Sect. 3.3). Guided by the work of Bremnes (2000) in comparing photometric mean values for field and group versus cluster dwarf irregulars, we adopted his slope of -0.08 found for Virgo and Centaurus cluster galaxies (Sect. 3.4). In an independent analysis of only the Virgo dwarf irregulars we find a slope about twice as steep. We checked that the structure-environment relation is present irrespective of the actually chosen slope value, as expected. For the inquiry on a linkage of photometric and kinematic data a steeper slope was used that emerged from double regression applied for reasons of statistical consistency (Sect. 3.6). Such a steeper slope also agrees better with a global $\log(\alpha_B^{-1}) - M_B$ relation as determined for a combined sample of late-type irregulars and early type spirals (Makarova 1999, her Fig. 5). We stress, however, that the qualitative results reported in this paper are insensitive to the adopted fitting procedure.

3.7.2. Origin of the structure-environment relation

The structure-environment relation says that for cluster dwarf irregulars the exponential parameters differ on average from those of non-cluster galaxies. In particular, the scale lengths for field and group dwarf irregulars are on average shorter and thus the central surface brightnesses are brighter than for dwarfs in clusters. This was already reported in Bremnes (2000) and in Paper VI and is confirmed here with our complete data sample (Sect. 3.4).

Several reasons may be responsible for the structure-environment relation. There are the manyfold influences of the cluster environment on a dwarf galaxy, including a relatively high peculiar velocity, galaxy harassment, ram pressure, and – quite important – tidal effects (stripping, stirring, induced angular momentum). In particular,

(i) an environmentally induced loss of a substantial amount of gas would lower the gravitational potential and thus expand the galaxy;

(ii) quenching of star-formation in cluster late-type galaxies may partly account for the observed effect. Late-type galaxies in clusters tend to be gas-deficient, implying a lowered present-day star formation rate (Gallagher & Hunter 1986; Cayatte et al. 1994). Thus Bremnes (2000) suggests a simple *uniform fading scenario* to explain the higher central surface brightness in field and group dwarf irregulars. According to this scenario star formation was much more efficient in cluster galaxies at earlier epochs while it is still ongoing at a moderately high rate in field and group galaxies. Such a fading in cluster irregulars would be accompagned by a reddening of the galaxies. Indeed, the cluster irregular sample of Gallagher & Hunter (1986) with $< B-V >= 0.51 \pm 0.02$ mag is by 0.11 ± 0.03 mag redder than their field and group comparison sample. This is also redder by 0.09 ± 0.03 mag than the equal means for the field and group irregular samples of Makarova (1999) and van Zee (2000), $< B-V >= 0.42 \pm 0.03$ mag. Consistently, Paper VI (excluding UGC 1281) provides us with a representative value of $< B-V >= 0.42 \pm 0.06$ mag for our sample of field and group dwarf irregular galaxies. The idea of quenched star-formation is additionally supported by our finding that for a given luminosity galaxies with higher scale lengths (or equivalently, with lower central surface brightnesses) are somewhat redder on average. This nicely agrees with the positive correlation between star formation or metallicity and central surface brightness in dwarf irregular galaxies as recently elucidated by van Zee (2001) and Grebel (2001), respectively. Thus both the colour trends that emerge from our photometric data (the sample mean colour values and the scale length dependence) provide some credits to a fading scenario;

(iii) due to tidal stirring, the initial gas dispersion of cluster dwarfs may be expected to be higher than in an isolated dwarf galaxy, naturally leading to a somewhat larger scale length for the stellar population (Andersen & Burkert 2000). Actually, tidal thickening of interacting galaxies has been observed by Reshetnikov & Combes (1997).

For low surface brightness dwarf galaxies Taylor (1997) observes an increased rate of star formation depending on the small-scale environment, thus empirically supporting the hypothesis that galaxy interactions may trigger bursts of star formation which lead in turn to structural transformations. Recent simulations on the evolution of group dwarf irregular galaxies orbiting *massive* galaxies even suggest morphological transformations, caused by tidal stirring, to either dwarf spheroidals or dwarf ellipticals (Mayer et al. 2001). Within the group galaxies of our sample such influences are, however, not (yet) manifest: for the parameters under investigation the group and field galaxies are rather similar (cf. Table 4). Our empirical finding of late-type spiral galaxies having on average not significantly shorter scale lengths than Im galaxies at similar absolute magnitudes neither validates nor contradicts such an evolutionary scenario, too. The scatter may simply be too large for such subtleties to be uncovered. This coincides with the negative result of Karachentsev et al. (1999) who state that their "tidal" or isolation index – which is a measure of local mass density surrounding a galaxy – is independent from the HI mass-to-luminosity ratio when applied to some hundred nearby galaxies of various types. Some hints for possible differences between our field and group data nevertheless arise from the slightly redder mean $B-R$ colour for group galaxies than for field galaxies, and from the smaller scatter for the group galaxies both in scale length at a given luminosity and in colour;

(iv) for field galaxies we observe a linkage between the optical parameters for an exponential disk and the dark matter contribution to the rotational velocity at an inner disk radius of about two scale lengths (Sect. 3.6). Concerning the structure-environment relation this linkage hints to the possibility that cluster galaxies are embedded in slightly different (more massive) halos than field galaxies resulting on average in somewhat higher disk scale

lengths. We discuss both our finding and its possible implication for the structure-environment relation further below (Sect. 3.7.4).

3.7.3. Change of colour gradients

Positive colour gradients are typical for most of our galaxies (see Fig. 9 b) and are naturally expected for galaxies with star formation concentrated to the denser inner regions. Despite of this, quite a few galaxies seem to have *negative* colour gradients. In particular, galaxies with scale lengths higher than about 1 kpc seem to enter the area of negative colour gradients. This is consistent with the observation that larger galaxies (LSB and normal spirals) have older central populations forcing negative colour gradients, with values correlated to bulge sizes (Bell & de Jong 2000; Matthews & Wood 2001; Andredakis et al. 1995). A handful of our dwarf irregular galaxies exhibit *strong negative* colour gradients, however. They all are faint, blue, and have relatively small scale lengths ($\alpha_B^{-1} \leq 0.6$ kpc). While particularly the appearance of young and small sized isolated galaxies may be strongly influenced by outward-propagating supershells which induce peripheral star formation activity, this seems unlikely to be the case for most of the galaxies under investigation. Thus the negative colour gradients neither seem to be related to heavily off-centered star formation sites dominating galaxy colour and structure nor can they be explained by an overtly red central stellar population. After inspection of the surface brightness profiles and the corresponding colour profiles, and taking care of the estimated errors, one comes to the conclusion that the strong negative gradients are photometric artefacts resulting from an inconsistent scale length determination in the two photometric bands which is propagated to the indirect gradient determinition method adopted; thus the gradients are likely to be much smaller, i.e. closer to zero, or even positive. This statement seems to hold for some galaxies with weakly negative colour gradients as well, particularly those with small scale lengths. An example for an unintended mismatch between gradient definition according to Eq. (6) and the actual colour profile as shown in Fig. 3 is UGCA 148 with similar scale lengths in B and R (as determined beyond $\approx 25''$) but with a relatively strong positive colour gradient in the outer envelope.

Strong positive colour gradients appear for galaxies with very short scale lengths only (see Fig. 9b) and – according to van Zee (2001) – may be related to starbursts. In fact, any centrally concentrated young population imprints its influence on the colour gradient more pronounced in a small galaxy (i.e. in one with relatively short scale lengths) than in a bigger galaxy. Moreover, *for galaxies with exponential intensity laws the colour gradients are positive and inversely proportional to the scale lengths in general as long as the blue-band scale lengths are shorter than those in the red band by a roughly constant value*. We have illustrated that adopting a scale length difference of about 10% will indeed approximately result in the expected behaviour for the majority of our galaxies. We have extracted this same behaviour from the data on isolated dwarf irregulars in van Zee (2001) and independently in Heller & Brosch (2001) for Virgo cluster dwarf irregulars. If a slightly more complicated factor of proportionality is allowed for, i.e. an affine relation as described, then galaxies with larger scale lengths are predicted to exhibit also negative colour gradients, as indeed is observed with our sample. There are two immediate consequences from such a behaviour. First, it implies *a constant $B-R$ colour increase of about 0.1 mag for an interval of one scale length for dwarf irregular galaxies, irrespective of size or total colour*. Second, the B-band scale lengths being systematically shorter than those in the R band (for the smaller galaxies only, i.e. those with short scale lengths) is in line with disk models that explain the formation and evolution of *exponential* gaseous and stellar systems by means of viscous radial infall (Firmani et al. 1996; Zhang & Wyse 2000; cf. also Hunter et al. 1998).

3.7.4. Kinematic couplings

The fair to tight correlations seen in Fig. 10 between optical disk parameters and the inferred accompagning disk dynamics are at first view rather astononishing, in particular for the rightmost panels given the crude estimate used for the input parameter v_0 of the Burkert model, i.e. $v_0 \approx 0.78\ v_{\rm rot}$. The quantitative results are, however, rather insensitive to the exact value of the adopted coefficient. Therefore it is not disturbing that the outermost observed rotational velocity of dwarf galaxies often resides on a still rising rotation curve and thus constitutes only a lower limit to the true maximum value where the rotation curve becomes flat. The tightness of the $\delta \log\ \alpha_B^{-1}$-$\delta \log\ v_{\rm h}$-relation is a consequence of applying the Burkert-model dark matter scaling relations at a small radius proportional to scale length: at small radii the imposed velocity profiles $v_{\rm h}(r)$ still form a rather similar family, thus reading off the velocities at scale-length dependent radii immediately translates into tightly correlated variations of circular velocity. Thus we are confident with our adopted working approximation and with the resulting correlations as presented.

Navarro (1997) already established an observational $\delta\mu_{0,i}^B$-$\delta \log\ v_{\rm h}$-like relation for high- and low-surface brightness galaxies working not with the Burkert-halo density distribution but with a Navarro-Frenk-White profile and having available measured rotational velocities at inner disk radii, particular at the peak rotational velocity. Recently, van den Bosch et al. (2001) studied the angular momentum content of dwarf galaxies with a sample of 14 late-type spirals. Using a Navarro-Frenk-White profile they determined the spin parameters for the baryonic disks. One can show that a – admittedly weak – correlation emerges from their data between either the central surface brightness or the scale length and the disk spin

parameter. Moreover, Chiba & Yoshi (1995) have already applied a tight correlation found between disk scale length and a combination of central surface brightness and measured rotational velocity at the characteristic radius of 2.14 scale lengths in order to determine extragalactic distances of early- and late-type spirals; their approach is similar to a Tully-Fisher relation study but working with inner disk circular velocities and assuming an exponential light distribution. This previous work and our own approach lead us to the conclusion that *the scatter in the scale length or surface brightness versus absolute magnitude diagrams, particularly for dwarf irregular galaxies, seems to be correlated with the kinematic disk properties induced by the surrounding dark matter halo.* The smaller kinematic contribution of luminous matter probably is related to the photometric structure as well, but due to the unknown disk mass-to-light ratios and ignoring effects of viscous infall we cannot make an argument as strong as above. Our conclusion is also in line with theoretical expectations: models on the formation of disk galaxies predict that, for a given mass or luminosity, increasing the halo angular momentum increases the exponential scale length or, correspondingly, decreases the extrapolated central surface brightness (Dalcanton et al. 1997; Zhang & Wyse 2000; Silk 2001). This applies to our case of measured rotional velocities, because halo angular momenta or halo circular speeds are indicative for the circular speed of the collapsed, centrifugally supported disks (Weil et al. 1998).

Accepting that higher-than-mean rotational velocities of field and group galaxies exhibit higher-than-mean scale lengths one wonders whether this trend should not show up in a direct comparison of the kinematics of cluster and field irregulars, too. This would point to a deeper cause for the structure-environment relation than a mere evolutionary difference, e.g. different halo populations. We are not aware of a study comparing observed rotational velocities in cluster and field environments in the sense that it supports or contradicts our interpretation; however, for galaxies in clusters Mould (1997) does not see a correlation of the intercept of the Tully-Fisher relation and cluster richness. Unfortunately, only 20 out of the 35 Virgo irregulars/late-type spirals mentioned in Sect. 3.7.1 do have kinematic data in the PGC, turning out to be too small a sample to exhibit the structure-environment shift. Thus we cannot rely on this cluster subsample in order to perform a kinematic analysis as above. Such a more complete and direct analysis is therefore postponed to future work with more galaxies at hand.

4. Summary and conclusions

The main contributions of this paper are:

- B- and R-band surface photometry for 25 Southern field dwarfs is presented, including the newly discoverd dwarf elliptical galaxy NGC 2784 DW1. An image gallery and the deduced surface brightness and colour profiles are shown; effective radii and surface brightnesses as well as the extrapolated central surface brightnesses and the scale lengths resulting from fitted exponential model profiles are listed. Total colors and formal color gradients are given.
- Our program of monitoring all dwarf galaxies in the nearby 10 Mpc volume is nearly completed, at least within a magnitude limit of $M_B \leq -14$ mag, allowing for a statistical exploitation.
- Im galaxies, late-type spirals, and BCD/BCD-like galaxies are indistinguishable as concerns their basic photometric parameter relations, and thus can be lumped together to form a homogenous class of galaxies ("irregulars").
- We introduce a clear-cut definition for the distinction of group and field galaxies: a group dwarf has a neighbour brighter than $M_B = -17.5$ mag within a distance of 1 Mpc.
- Our previously (Paper VI) claimed statistical dependence of structure on large-scale galaxy environment, the structure-environment relation, is confirmed for the dwarf irregulars: at a given luminosity a much denser environment is related to a higher mean scale length or fainter mean central surface brightness, and to sligthly redder $B-R$ colours. See Bremnes (2000) for a similar finding concerning dwarf ellipticals.
- Group dwarfs obey the same structure-environment relation as field dwarfs.
- There seems to be a systematic trend from dwarf irregulars with shorter to longer scale lengths (i.e. from smaller/fainter to bigger/brighter galaxies) to change from positive to neglectable and even negative $B-R$ colour gradients.
- Dwarf irregulars exhibit a mean outward reddening $B-R$ of about 0.1 mag after one scale length or 0.16 mag after one kpc.
- For an individual dwarf irregular galaxy at a given luminosity the scatter in scale length or surface brightness is related to the kinematics of the galaxy's inner disk: a larger-than-mean scale length or fainter-than-mean central surface brightness is correlated with a faster-than-mean rotational velocity of the halo contribution at an inner disk radius of about two scale lengths; this is no more seen if circular velocity is measured at large radii where baryonic matter has lost dynamic importance.
- This structure-dynamics relation describing a linkage between photometric and kinematic properties has to be confirmed by means of a sample of galaxies with resolved velocity curves. If verified it may account for the structure-environment relation provided there is also a dynamics-environment relation, i.e. a systematic difference between the halos of cluster and field galaxies. This needs to be investigated.

Acknowledgements. B.R.P. thanks Markus Samland, Victor Debattista, and Alfonso Aguerri for stimulating conversations. Financial support by the Swiss National Science Foundation

is gratefully acknowledged. This work has made use of the NASA/IPAC Extragalactic Database (NED) which is operated by the Jet Propulsion Laboratory, CalTech, under contract with NASA and NASA's ADS Abstract Service.

References

Andersen, R.-P., & Burkert, A. 2000, ApJ, 531, 296
Andredakis, Y. C., Peletier, R. F., & Balcells, M. 1995, MNRAS, 275, 874
Barazza, F. D., Binggeli, B., & Prugniel, P. 2001, A&AS, 373, 12 (Paper VI)
Bell, E., & de Jong, R. S. 2000, MNRAS, 312, 497
Bergvall, N., Rönnback, J., Masegosa, J., & Östlin, G. 1999, A&A, 341, 697
Binggeli, B., & Cameron, L. M. 1993, A&AS, 98, 297
Bottinelli, L., Gouguenheim, L., Fouqué, P., & Paturel, G. 1990, A&AS, 82, 391
Bremnes, T. 2000, Ph.D. Thesis, Universität Basel
Bremnes, T., Binggeli, B., & Prugniel, P. 1998, A&AS, 129, 313 (Paper I)
Bremnes, T., Binggeli, B., & Prugniel, P. 1999, A&AS, 137, 337 (Paper III)
Bremnes, T., Binggeli, B., & Prugniel, P. 2000, A&AS, 141, 211 (Paper IV)
Bureau, M., Freeman, K. C., Pfitzner, D. W., & Meurer, G. R. 1999, AJ, 118, 2158
Burkert, A. 1995, ApJ, 447, L25
Cayatte, V., Kotanyi, C., Balkowski, C., & van Gorkom, J. H. 1994, AJ, 107, 1003
Carignan, C., & Freeman, K. C. 1988, ApJ, 332, L33
Chiba, M., & Yoshi, Y. 1995, ApJ, 442, 82
Côté, S. 1995, Ph.D. Thesis, Australian National University, Canberra
Côté, S., Freeman, K. C., Carignan, C., & Quinn, P. J. 1997, AJ, 114, 1313
Dalcanton, J. J., Spergel, D. N., & Summers, F. J. 1997, ApJ, 482, 659
De Vaucouleurs, G. 1959, Handbuch der Physik, ed. S. Flügge (Springer, Berlin), 53 275
De Vaucouleurs, G., De Vaucouleurs, A., Corwin, J. R., et al. 1991, RC3, C
Ferguson, H. C., & Sandage, A. 1990, AJ, 100, 1
Firmani, C., Hernandez, X., & Gallagher, J. 1996, A&A, 308, 403
Freeman, K. C. 1970, ApJ, 160, 811
Gallagher, J. S., & Hunter, D. A. 1986, AJ, 92, 557
Graham, A. W., & de Blok, W. J. G. 2001, ApJ, 556, 177
Grebel, E. K. 2001, in Dwarf Galaxies and their Environment, Conf. Proc., ed. K. de Boer, R.-J. Dettmar, & U. Klein (University of Bonn), 45
Haynes, M. P., Hogg, D. E., Maddalena, R. J., Roberts, M. S., & van Zee, L. 1998, AJ, 115, 62
Heller, A. B., & Brosch, N. 2001, MNRAS, 327, 80
Hubble, E. 1926, ApJ, 64, 321
Huchtmeier, W. K., Karachentsev, I. D., Karachentseva, V. E., & Ehle, M. 2000, A&AS, 141, 469
Hunter, D. A., Elmegreen, B. G., & Baker, A. L. 1998, ApJ, 493, 595
Isobe, T., Feigelson, E. D., Akritas, M. G., & Babu, G. J. 1990, ApJ, 364, 104
Jerjen, H., & Dressler, A. 1997, A&AS, 124, 1
Karachentsev, I. D., & Makarov, D. I. 1999, in Galaxy Interactions at Low and high Redshift, IAU Symp., ed. J. E. Barnes, & D. B. Sanders (Kluwer: Dordrecht), 109
Karachentsev, I. D., Makarov, D. I., & Huchtmeier, W. K. 1999, A&AS, 139, 97
Karachentsev, I. D., Karachentseva, V. E., Kudrya, Y. N., Sharina, M. E., & Parnovsky, S. L. 1999, AISAO, 3K
Karachentsev, I. D., Sharina, M. E., Grebel, E. K., et al. 2000, ApJ, 542, 128
Kraan-Korteweg, R. C., & Tammann, G. A. 1979, Astron. Nachr., 300, 181
Kunth, D., & Östlin, G. 2000, A&ARv, 10, 1
Landolt, A. U. 1992, AJ, 104, 340
Makarova, L. 1999, A&AS, 139, 491
Matthews, L. D., & Wood, K. 2001, ApJ, 548, 150
Marlowe, A. T., Meurer, G. R., & Heckman, T. M. 1999, ApJ, 522, 183
Mayer, L., Governato, F., Colpi, M., Moore, B., & Quinn, T. 2001, ApJ, 547, L123
Meurer, G. R., Mackie, G., & Carignan, C. 1994, AJ, 107, 2021
Mould, J. 1997, in Galaxy Scaling Relations, ed. L. N. da Costa & A. Renzini, ESO Astrophys. Symp. (Springer-Verlag), 170
Navarro, J. F. 1997, in ASP Conf. Ser., ed. M. Persic, & P. Salucci, 117, 404
Paturel, G., Fouque, P., Bottinelli, L., & Gouguenheim, L. 1992, Catalogue of Principal Galaxies, Lyon (PGC)
Puzia, T. H., Kissler-Patig, M., Brodie, J. P., & Schroder, L. L. 2000, AJ, 120, 777
Reshetnikov, V., & Combes, F. 1997, in Galaxy Scaling Relations, ed. L. N. da Costa & A. Renzini, ESO Astrophys. Symp. (Springer-Verlag), 387
Salucci, P., & Burkert, A. 2000, ApJ, 537, L9
Sandage, A., & Binggeli, B. 1984, AJ, 89, 919
Schlegel, D. J., Finkbeiner, D. P., & Davis, M. 1998, ApJ, 500, 525
Seitzer, P., Grebel, E. K., Dolphin, A. E., et al. 2001, Bull. AAS, 198, #09.09
Silk, J. 2001, MNRAS, 324, 313
Simpson, C. E., & Gottesman, S. T. 2000, AJ, 120, 2975
Sung, E.-C., Han, C., Ryden, B. S., et al. 1998, ApJ, 505, 199
Taylor, C. L. 1997, ApJ, 480, 524
Tully, B., & Fouqué, P. 1985, ApJS, 58, 67
Van den Bosch, F. C., Burkert, A., & Swaters, R. A. 2001, MNRAS, 326, 1205
Van Zee, L. 2000, AJ, 119, 2757
Van Zee, L. 2001, AJ, 121, 2003
Weil, M. L., Eke, V. R., & Efstathiou, G. 1998, MNRAS, 300, 773
Zhang, B., & Wyse, R. F. G. 2000, MNRAS, 313, 310